Loss of tolerance to multiple environmental stresses due to limitation of structural diversity of complex sphingolipids

Ayano Koga[a], Chihiro Takayama[a], Yohei Ishibashi[b], Yushi Kono[a], Momoko Matsuzaki[a], and Motohiro Tani[a,*]

[a]Department of Chemistry, Faculty of Sciences, and [b]Department of Bioscience and Biotechnology, Graduate School of Bioresource and Bioenvironmental Sciences, Kyushu University, Nishi-ku, Fukuoka 819-0395, Japan

ABSTRACT **Structural diversity of complex sphingolipids is important for maintenance of various cellular functions; however, the overall picture of the significance of this structural diversity remains largely unknown. To investigate the physiological importance of the structural diversity of complex sphingolipids, we here constructed a complex sphingolipid structural diversity disruption library in budding yeast, which comprises 11 mutants including with combinations of deletions of sphingolipid-metabolizing enzyme genes. The sensitivity of the mutants to various environmental stresses revealed that the more the structural variation of complex sphingolipids is limited, the more stress sensitivity tends to increase. Moreover, it was found that in mutant cells with only one subtype of complex sphingolipid, Slt2 MAP kinase and Msn2/4 transcriptional factors are essential for maintenance of a normal growth and compensation for reduced tolerance of multiple stresses caused by loss of complex sphingolipid diversity. Slt2 and Msn2/4 are involved in compensation for impaired integrity of cell walls and plasma membranes caused by loss of complex sphingolipid diversity, respectively. From these findings, it was suggested that loss of structural diversity of complex sphingolipids affects the environment of the cell surface, including both plasma membranes and cell walls, which could cause multiple environmental stress hypersensitivity.**

Monitoring Editor
Robert Parton
University of Queensland

Received: Apr 7, 2022
Revised: Jun 27, 2022
Accepted: Jul 20, 2022

INTRODUCTION

Biological membranes are based on a lipid bilayer composed of a wide variety of membrane lipids, and the structural diversity of these membrane lipids is considered to be an important factor that supports the multifunctions of biological membranes, such as signal transduction, transport of various molecules, and acquirement of stress tolerance. Complex sphingolipids, one of the classes in eukaryotic biomembranes, exhibit particularly complex structural diversity among membrane lipids. In mammals, complex sphingolipids have hundreds of hydrophilic head groups, and structural variation in long-chain bases (LCBs) and fatty acids in the ceramide (Cer) moiety of complex sphingolipids further complicates their structural diversity (Merrill, 2011). Although the overall picture of the significance of the structural diversity of complex sphingolipids in a single organism remains largely unknown, several lines of evidence have suggested the physiological significance of the structural diversity of complex sphingolipids in mammals; for example, the knockout mouse as to the lactosylCer α-2,3-sialyltransferase gene knockout mouse, which is responsible for the biosynthesis of glycosphingolipid GM3, exhibits altered sensitivity to insulin and complete hearing loss (Yamashita *et al.*, 2003; Yoshikawa *et al.*, 2009). However, establishment of mammalian cells having only one subtype of complex sphingolipids, which will be an effective means to understand the significance of the structural diversity, has not been

This article was published online ahead of print in MBoC in Press (http://www.molbiolcell.org/cgi/doi/10.1091/mbc.E22-04-0117) on July 27, 2022.

Conflict of interest: The authors declare no conflict of interest.

Author contributions: M.T. and A.K. conceived and coordinated the study and wrote the paper. A.K. and M.T. designed and performed the analysis presented in Figures 1–8. C.T. performed the analysis presented in Figure 2. Y.I. performed the LC-ESI MS/MS analysis. Y.K. performed the analysis presented in Figure 7. M.M. was involved in generation of the mutant cells used in this study.

*Address correspondence to: Motohiro Tani (tani@chem.kyushu-univ.jp).

Abbreviations used: Cer, ceramide; CFW, calcofluor white; CWI, cell wall integrity; Dox, doxycycline; GO, gene ontology; HOG, high osmolarity glycerol; IPC, inositol phosphorylceramide; LCB, long chain base; MIPC, mannosylinositol phosphorylceramide; $M(IP)_2C$, mannosyldiinositol phosphorylceramide; SPT, serine palmitoyltransferase.

© 2022 Koga *et al.* This article is distributed by The American Society for Cell Biology under license from the author(s). Two months after publication it is available to the public under an Attribution–Noncommercial-Share Alike 4.0 International Creative Commons License (http://creativecommons.org/licenses/by-nc-sa/4.0).

"ASCB®," "The American Society for Cell Biology®," and "Molecular Biology of the Cell®" are registered trademarks of The American Society for Cell Biology.

reported, because the limitation of the diversity requires very complicated genetic manipulations.

The structural diversity of complex sphingolipids in budding yeast *Saccharomyces cerevisiae* is relatively simple as compared with that in mammals. This is mainly because the fatty acid chain length in the Cer moiety is mainly limited to C26 and complex sphingolipids in budding yeast have only three types of hydrophilic head group consisting of inositol phosphate and mannose (Dickson and Lester, 2002; Dickson *et al.*, 2006; Tani, 2016). Owing to differences in hydrophilic structure, yeast complex sphingolipids are divided into inositol phosphorylceramide (IPC), mannosylinositol phosphorylceramide (MIPC), and mannosyldiinositol phosphorylceramide ($M(IP)_2C$) (Figure 1, A and B) (Dickson and Lester, 2002; Dickson *et al.*, 2006; Tani, 2016). In addition, the Cer moiety in complex sphingolipids can be classified into five types (types A, B, B′, C, and D) according to the hydroxylation state (Figure 1, A and B) (Dickson and Lester, 2002; Dickson *et al.*, 2006; Tani, 2016). Thus, 15 subtypes of complex sphingolipids can be synthesized in budding yeast (Figure 1, A and B) (Tani, 2016). The structural diversity of complex sphingolipids in budding yeast is determined by five sphingolipid-metabolizing enzyme proteins, which are involved in extension of the hydrophilic head group (MIPC synthases Sur1 [Csg1] and Csh1 and $M(IP)_2C$ synthase Ipt1) and hydroxylation of the Cer moiety (sphingolipid C4-hydroxylase Sur2 and sphingolipid α-hydroxylase Scs7) (Figure 1, A and B) (Beeler *et al.*, 1997; Dickson *et al.*, 1997; Haak *et al.*, 1997; Uemura *et al.*, 2003). So far, it has been reported that deletion of any of these genes causes various abnormal phenotypes. Deletion of Csg1 and Csh1, which causes complete loss of MIPC biosynthesis, causes hypersensitivity to Ca^{2+} and low pH conditions (Uemura *et al.*, 2003; Otsu *et al.*, 2020), impairment of cell wall integrity and endosomal trafficking (Tani and Kuge, 2012b; Morimoto and Tani, 2015; Tanaka and Tani, 2018), and reduction of cell viability under nitrogen starvation (Yamagata *et al.*, 2013; Knupp *et al.*, 2017). The detrimental effect of loss of MIPC biosynthesis on sensitivity to Ca^{2+}, low pH, or nitrogen starvation is not due to loss of MIPCs itself, but to the abnormal accumulation of IPCs, the precursor of MIPCs (Zhao *et al.*, 1994; Yamagata *et al.*, 2013; Knupp *et al.*, 2017; Otsu *et al.*, 2020). Several lines of evidence also suggest the importance of *SUR2, SCS7,* or *IPT1*. For instance, hydroxylation of the LCB moiety by *SUR2* is required for formation of a lateral diffusion barrier in the endoplasmic reticulum (ER) between mother and daughter cells (Clay *et al.*, 2014). *IPT1* and *SCS7* are essential for maintenance of normal cell growth when expression of phosphatidylserine (PS) synthase is repressed (Tani and Kuge, 2010b; Toda *et al.*, 2020), indicating that the detailed structural features of complex sphingolipids determined by these genes are important when PS biosynthesis is repressed. In addition, it was also reported that deletion of *IPT1* or *SCS7* affects the sensitivities to some drugs (Hallstrom *et al.*, 2001; Herrero *et al.*, 2008).

The information as to which structural deficiency of complex sphingolipids causes what kind of abnormality is somewhat fragmentary even in budding yeast. For example, in high-throughput analysis, abnormal phenotypes caused by limitation of the structural diversity of complex sphingolipids are the result of a single deletion of a sphingolipid-metabolizing enzyme including MIPC synthases, $M(IP)_2C$ synthase, and sphingolipid hydroxylases (Dudley *et al.*, 2005; Mira *et al.*, 2010). Thus, there is not much information on the phenotypes caused by more severe disruption of the structural diversity due to the combination of deletion of multiple enzymes, for example, simultaneous defects of structural diversity of both the hydrophilic head group and the Cer moiety. In addition, budding yeast has two MIPC synthases, Csg1 and Csh1, and MIPC biosynthesis is not abolished completely with only one of the deletions (Uemura *et al.*, 2003). Also, upon single deletion of *CSG2* encoding the regulatory subunit of Csg1 and Csh1, a trace biosynthesis of MIPC still occur (Uemura *et al.*, 2003; Tani and Kuge, 2012b). Furthermore, it was also shown that the abnormal phenotype caused by the single deletion of the gene involved in MIPC biosynthesis was weaker than that on double deletion of *CSG1* and *CSH1*, which causes complete loss of MIPC biosynthesis (Morimoto and Tani, 2015; Otsu *et al.*, 2020). Here, to systematically investigate the physiological importance of the structural diversity of complex sphingolipids, we created a complex sphingolipid structural diversity disruption library in budding yeast, which comprises mutants with various combinations of deletions of *CSG1*, *CSH1*, *SUR2*, *SCS7*, and *IPT1* (Figure 1C). Analyses of this library revealed that, under various environmental stresses, the more the structural variation of both the hydrophilic group and the Cer moiety is limited, the more stress sensitivity tends to increase. Furthermore, it was found that mutant cells with only one subtype of complex sphingolipid exhibit impairment of both cell walls and plasma membranes, and these cell surface environment defects could be one of the causes of hypersensitivity to multiple environmental stresses due to the defect of structural diversity of complex sphingolipids.

RESULTS

Construction of a complex sphingolipid structural diversity disruption library

In *S. cerevisiae*, 15 subtypes of complex sphingolipid can be synthesized in total, the structural diversity being created by five sphingolipid-metabolizing enzymes, Csg1, Csh1, Sur2, Scs7, and Ipt1 (Figure 1, A and B). To systematically investigate the physiological importance of the structural diversity of complex sphingolipids, we constructed a complex sphingolipid diversity disruption library in budding yeast that comprises 11 mutants with various combinations of deletions of *CSG1*, *CSH1*, *SUR2*, *SCS7*, and *IPT1* (Figure 1C). As shown in Figure 1D, the expected disappearance of specific subtypes of complex sphingolipid was observed in each library mutant; for example, in *sur2*Δ *scs7*Δ (*ss*Δ) or *csg1*Δ *csh1*Δ (*cc*Δ) cells, hydroxylated complex sphingolipids (B, B′, C, and D types) or MIPCs and $M(IP)_2Cs$ disappeared, respectively. Moreover, in *csg1*Δ *csh1*Δ *sur2*Δ *scs7*Δ (*ccss*Δ) cells, only one subtype (IPC-A) was detected (Figure 1D). The total amount of complex sphingolipids was not significantly different among the wild-type, *cc*Δ, *ss*Δ, *ccss*Δ, *ipt1*Δ, and *ipt1*Δ *sur2*Δ *scs7*Δ *(ipt1*Δ *ss*Δ) cells (Figure 1E). The results for *ss*Δ, *cc*Δ, and *ccss*Δ cells were consistent with those of a previous report (Uemura *et al.*, 2014). Liquid chromatography-electrospray ionization-tandem mass spectrometry (LC-ESI MS/MS) analysis of free Cers revealed that the carbon chain lengths of fatty acid and LCB in Cers in wild-type, *ss*Δ, *cc*Δ, *ccss*Δ, *ipt1*Δ, and *ipt1*Δ *ss*Δ cells are mainly C26 and C18, respectively (Figure 1F), which is likely to reflect the composition of the Cer moiety of complex sphingolipids. Thus, it was suggested that the loss of biosynthesis of MIPCs and $M(IP)_2Cs$ and/or hydroxylation of the Cer moiety do not dramatically affect the carbon chain length of the Cer moiety. Although significant differences in the complex sphingolipid levels were not observed between these mutant cells (Figure 1E), a decrease in the total amount of Cers was observed in *ss*Δ and *ipt1*Δ *ss*Δ cells, but not in *cc*Δ and *ccss*Δ cells (Figure 1F). The levels of phosphatidylcholine (PC), phosphatidylserine/phosphatidylinositol (PS/PI), and phosphatidylethanolamine (PE) in *ss*Δ, *cc*Δ, *ccss*Δ, *ipt1*Δ, and *ipt1*Δ *ss*Δ cells did not change as compared with wild-type cells (Supplemental Figure S1), indicating that the alteration of the structural diversity of complex sphingolipids does not affect cellular levels of major

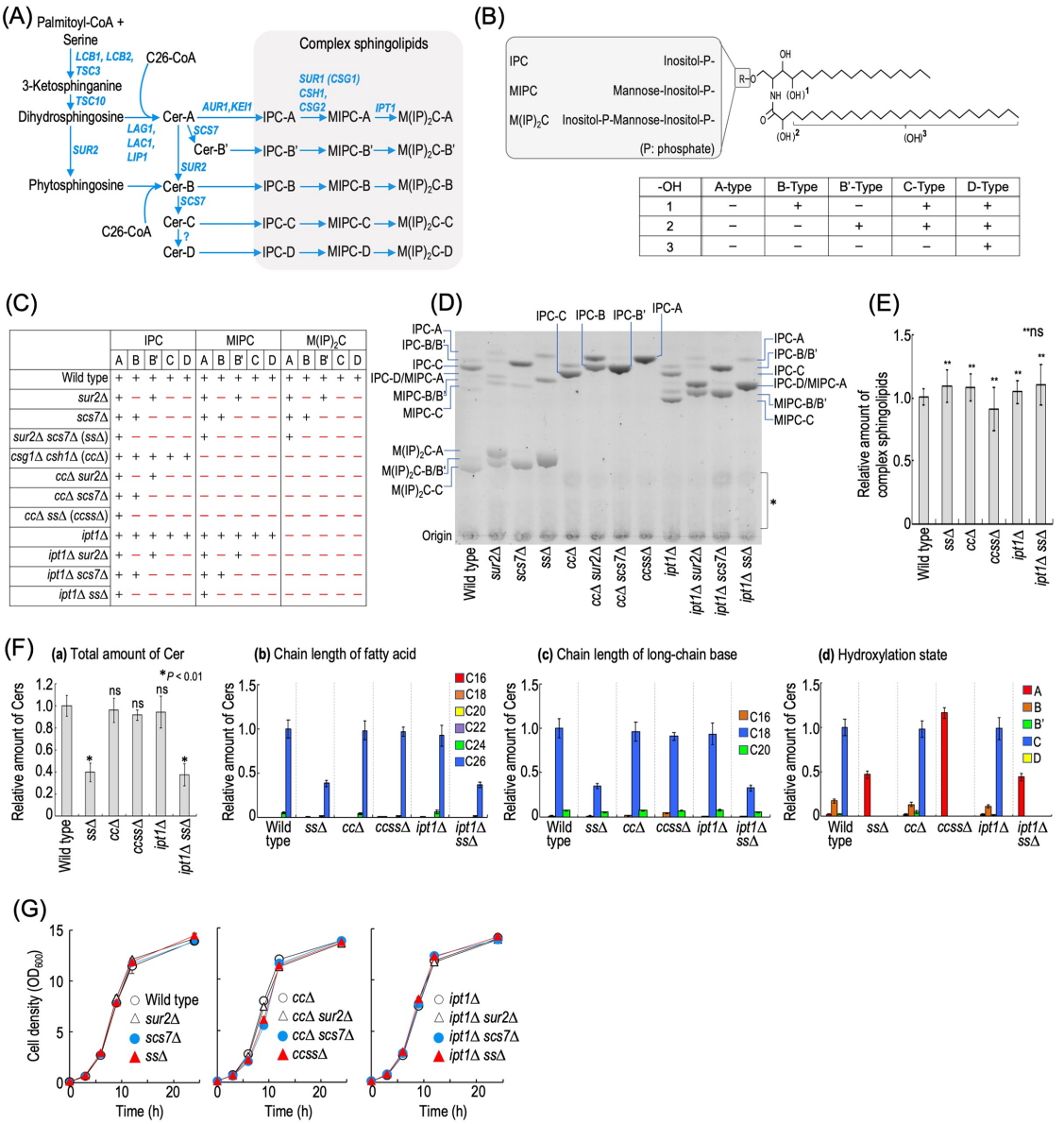

FIGURE 1: Construction of a complex sphingolipid structural diversity disruption library. (A) Complex sphingolipid biosynthesis pathway in budding yeast *S. cerevisiae*. The pathway and genes responsible for the synthesis of complex sphingolipids in *S. cerevisiae* are shown. Owing to the different hydrophilic head groups and hydroxylation states of the ceramide (Cer) moiety, 15 subtypes of complex sphingolipid can be synthesized. For convenience, *SUR1* encoding MIPC synthase is called *CSG1* in this study. (B) Structure of *S. cerevisiae* complex sphingolipids. *S. cerevisiae* complex sphingolipids have three types of hydrophilic head group. Hydroxylation sites in the Cer moiety are labeled 1, 2, and 3. Sites 1 (the C-4 position of LCBs) and 2 (the C-2 position in fatty acids) are hydroxylated by Sur2 and Scs7, respectively. Site 3 is at an unknown position on the fatty acids, and the enzyme involved in the hydroxylation has not yet been identified. Owing to the difference in hydroxylation state, the Cer moiety of complex sphingolipids is classified into the A, B, B′, C, and D types. (C) The structural diversity of complex sphingolipid-disrupted mutants used in this study. A plus symbol indicates a subtype of complex sphingolipids that can be synthesized in each type of mutant cells. (D) TLC analysis of the mutant cells. Cells were cultured overnight in YPD medium, diluted (0.3 OD_{600} units/ml) in fresh YPD medium, and then incubated for 5 h at 30°C. Lipids were extracted, subjected to mild alkaline treatment, separated by TLC, and then visualized with a copper sulfate and orthophosphoric acid reagent. The asterisk indicates unidentified bands. (E) Amounts of complex sphingolipids in wild-type (MTY174), *sur2Δ scs7Δ* (*ssΔ*), *csg1Δ csh1Δ* (*ccΔ*), *csg1Δ csh1Δ sur2Δ scs7Δ* (*ccssΔ*), *ipt1Δ*, and *ipt1Δ sur2Δ scs7Δ* (*ipt1Δ ssΔ*) cells. TLC analysis was performed as described in D. The amount of complex sphingolipids (IPCs, MIPCs, and $M(IP)_2Cs$) in wild-type cells was taken as 1. (F) Analysis of free Cers by LC-ESI MS/MS. Cells were cultured, and lipids were extracted as described in D. Cers were measured by the MRM mode constructed by the combination of LCBs and fatty acids with different chain lengths or hydroxylation states. The total amount of Cers (panel a), carbon chain lengths of the fatty acid moieties (panel b), carbon chain lengths of the LCB moieties (panel c), and hydroxylation state of Cers (panel d) are shown. (G) Time course of cell growth. Cells were cultured overnight in YPD medium at 30°C and diluted (0.1 OD_{600} units/ml) in fresh YPD medium, and then aliquots of the cell suspensions were subjected to cell density measurements (OD_{600}) at the indicated times. Data represent means ± SD for one experiment (triplicate) representative of three independent experiments. ns: no significant difference. The details are given in *Materials and Methods*.

glycerophospholipids. Although the growth rates of *ccss*Δ and *cc*Δ *scs7*Δ cells in YPD medium were slightly lower than that of wild-type cells, there was no significant difference for other mutants (Figure 1G), indicating that defects of the structural diversity of complex sphingolipids do not have a serious effect on cell growth under normal conditions. However, when the carbon source was changed from glucose to glycerol/ethanol, the growth of *cc*Δ, *cc*Δ *sur2*Δ, *cc*Δ *scs7*Δ, and *ccss*Δ cells was decreased (Supplemental Figure S2). Furthermore, on changing to lactic acid, a decrease in the growth of the *ccss*Δ strain was also clearly observed (Supplemental Figure S2). In contrast, such a difference of growth among mutants was not observed under anaerobic conditions (Supplemental Figure S2). These results suggested that these mutations have a marked effect on respiratory growth.

Defect of tolerance of various environmental stresses due to defects of the structural diversity of complex sphingolipids

It has been reported that yeast cells with impaired structural diversity of complex sphingolipids exhibit increased sensitivity to cell wall–related stresses, low pH, metal ions, and some drugs (Zhao *et al.*, 1994; Hallstrom *et al.*, 2001; Herrero *et al.*, 2008; Morimoto and Tani, 2015; Tanaka and Tani, 2018; Otsu *et al.*, 2020). Here, by using the complex sphingolipid disruption library, we investigated which structural deficiencies of complex sphingolipids affect what kind of environmental stresses, including those previously reported (Figure 2). MIPC biosynthesis–deficient cells (*cc*Δ cells in this study), which have been most frequently reported as mutants showing various abnormal phenotypes among mutants included in the library, exhibited increased sensitivity to NaCl, KCl, acetic acid (pH 5.5), pH 3.5, caffeine, SDS, hydroxyurea, zeocin, $CuCl_2$, $CdCl_2$, and $CaCl_2$. In contrast, deletion of *SUR2, SCS7*, or both (*ss*Δ) did not have marked effects as compared with *cc*Δ; however, when these mutations were combined with *cc*Δ (*ccss*Δ, *cc*Δ *sur2*Δ, and *cc*Δ *scs7*Δ), they had synergistic effects on stress sensitivity. That is, for 40°C, NaCl, KCl, organic acids (acetic acid, sorbic acid, and benzoic acid), pH 8.0, SDS, cycloheximide, and zeocin, *ccss*Δ cells were more sensitive than *cc*Δ or *ss*Δ cells. Conversely, it was also observed that the deletion of *SUR2* and/or *SCS7* suppressed the increased sensitivity due to *cc*Δ; that is, the hypersensitivity to pH 3.5, $CaCl_2$, or $CuCl_2$ due to *cc*Δ was partly recovered on deletion of *SUR2* or *SCS7* (*cc*Δ vs. *cc*Δ *sur2*Δ or *cc*Δ *scs7*Δ cells). The recovery of sensitivity to $CdCl_2$ was observed only in *cc*Δ *sur2*Δ cells. The recovery of sensitivity to pH 3.5 or $CaCl_2$ was also observed in *ccss*Δ cells. The suppressive effect of *sur2*Δ or *scs7*Δ on the hypersensitivity to pH 3.5 or $CaCl_2$ due to *cc*Δ was consistent with previous reports (Tani and Toume, 2015; Otsu *et al.*, 2020). As compared with wild-type cells, *cc*Δ cells exhibited resistance to calcofluor white (CFW), which binds to chitin at the cell wall and subsequently perturbs the function of the cell wall (Ram and Klis, 2006); however, the effect of this resistance was reduced in *ccss*Δ cells (this will be discussed later). For $M(IP)_2C$ biosynthesis–deficient mutants (*ipt1*Δ, *ipt1*Δ *sur2*Δ, *ipt1*Δ *scs7*Δ, and *ipt1*Δ *ss*Δ cells), there was very little change in stress sensitivities as compared with the MIPC biosynthesis–deficient mutants (Figure 2). Overall, these results indicated that most of the stress hypersensitivity due to limitation of structural diversity of complex sphingolipids is mainly caused by the loss of biosynthesis of MIPCs, but not $M(IP)_2Cs$, and the loss of hydroxylation in the Cer moiety promotes or suppresses the detrimental effects due to loss of MIPC biosynthesis. Notably, it was also indicated that *ccss*Δ cells having only one subtype of complex sphingolipid are the most severely sensitive to the majority of stresses.

Abnormal phenotypes due to accumulation of IPCs or disappearance of MIPC and $M(IP)_2C$

It was reported that hypersensitivity to Ca^{2+} or low pH due to a defect of MIPC biosynthesis is suppressed not only by the deletion of *SUR2* or *SCS7* but also by suppression of de novo sphingolipid biosynthesis, which includes inhibition of serine palmitoyltransferase (SPT) (Zhao *et al.*, 1994; Otsu *et al.*, 2020) (Figure 1A). This implies that excess accumulation of IPCs, precursors of MIPCs, triggers these abnormal phenotypes in MIPC biosynthesis–deficient cells. Next, we examined how the various stress sensitivities seen in *cc*Δ cells were altered by inhibition of the de novo sphingolipid biosynthesis pathway. To repress de novo biosynthesis of all sphingolipids, myriocin, an inhibitor of SPT, was used. As shown in Figure 3A, treatment with 0.1 μg/ml myriocin significantly reduced the complex sphingolipid levels in both wild-type and *cc*Δ cells. We also used a mutant strain that carries the *LIP1* gene encoding the regulatory subunit of Cer synthases under the control of a tetracycline-regulatable (Tet) promoter (*tet-LIP1*) for repression of biosynthesis of Cers (Supplemental Figure S3) (Tani and Kuge, 2010a; Toume and Tani, 2016). *tet-LIP1* and *tet-LIP1 cc*Δ cells also exhibited a decrease in complex sphingolipid levels when they were treated with doxycycline (Dox), which represses expression of the gene under the Tet promoter (Supplemental Figure S3A). As reported previously, under these de novo sphingolipid biosynthesis–repressive conditions, hypersensitivity to pH 3.5 or $CaCl_2$ due to *cc*Δ was suppressed (Figure 3B and Supplemental Figure S3B). However, the sensitivities to $CuCl_2$, NaCl, acetic acid, SDS, and caffeine in *cc*Δ cells were promoted by both myriocin treatment and *LIP1* repression, or either, suggesting that hypersensitivity to these stresses is not caused by the accumulation of IPCs, but probably by loss of MIPCs (and also $M(IP)_2Cs$) (Figure 3B and Supplemental Figure S3B). It should be noted that $CuCl_2$ hypersensitivity due to *cc*Δ was suppressed by *scs7*Δ or *sur2*Δ (Figure 2), suggesting that the rescue mechanism through a defect of hydroxylation in the Cer moiety is not necessarily associated with the rescue mechanism through avoidance from accumulation of IPCs. Collectively, these results indicated that the abnormal phenotypes due to the loss of biosynthesis of MIPC are caused by multiple factors. In addition, the hypersensitivities to $CuCl_2$, NaCl, acetic acid, SDS, and caffeine due to *ccss*Δ were also promoted or unaffected by myriocin treatment or *LIP1* repression (Supplemental Figure S4), suggesting that, in *ccss*Δ cells, the hypersensitivities to these stresses are not also caused by accumulation of IPC-A.

Relationship between multiplestress hypersensitivity and stress response systems in *ccss*Δ cells

Yeast cells have a variety of stress responsive signal transduction systems to compensate for their growth under stress, and thus it was assumed that the multiplestress hypersensitivity of complex sphingolipid diversity–deficient cells is caused by impairment of stress response system(s). Therefore, we examined the stress sensitivity of *ss*Δ, *cc*Δ, and *ccss*Δ cells in the absence of the typical stress response systems. Because *ccss*Δ cells exhibited hypersensitivity to NaCl and alkaline pH, Hog1 MAP kinase in the high-osmolarity glycerol (HOG) pathway (Brewster and Gustin, 2014) or alkaline pH–responsive transcription factor Rim101 in the Rim pathway (Futai *et al.*, 1999) was deleted. In addition, because altered sensitivity to CFW, SDS, and caffeine may imply an abnormality in cell wall integrity (Levin, 2005; Ram and Klis, 2006), Slt2 MAP kinase in the cell wall integrity (CWI) pathway was also deleted. As shown in Figure 4, A and B, *ccss*Δ caused hypersensitivity to NaCl and sorbitol or alkaline pH in the absence of Hog1 or Rim101, respectively (*hog1*Δ vs. *ccss*Δ *hog1*Δ

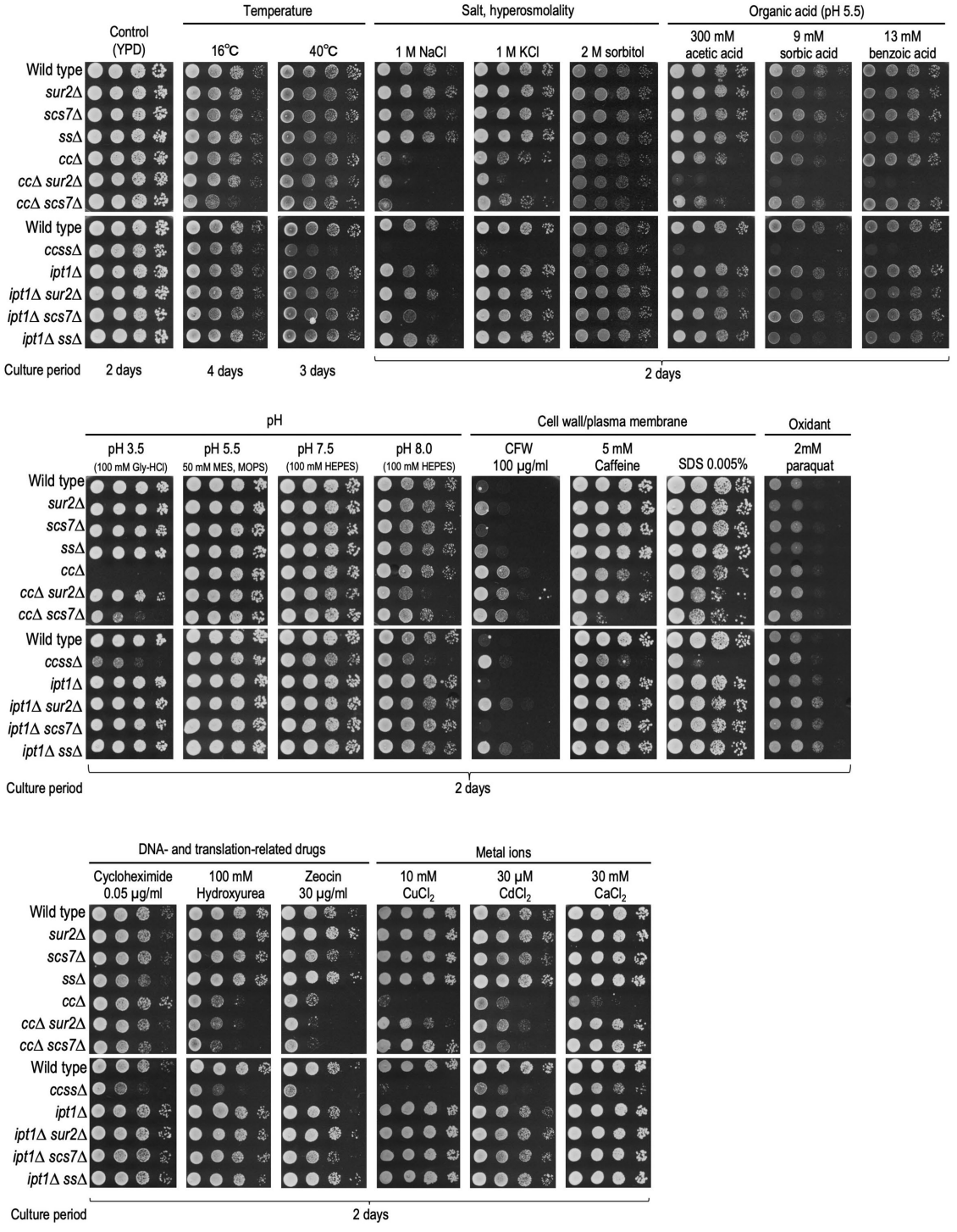

FIGURE 2: Sensitivities of the complex sphingolipid structural diversity disruption library to various stress conditions and different carbon sources. Cells cultured overnight in YPD medium at 30°C were spotted onto agar plates containing the indicated compounds: YPD containing 1 M NaCl, 1 M KCl, 2 M sorbitol, 100 µg/ml CFW, 5 mM caffeine, 0.005% SDS, 2 mM paraquat, 0.05 µg/ml cycloheximide, 100 mM hydroxyurea, 30 µg/ml zeocin, 10 mM $CuCl_2$, 30 µM $CdCl_2$, or 30 mM $CaCl_2$; YPD buffered with 100 mM Gly-HCl (for pH 3.5), 50 mM MES and MOPS (for pH 5.5), or 100 mM HEPES (for pH 7.5 and 8.0); YPD buffered at pH 5.5 by the addition of 50 mM MES and MOPS, and containing 300 mM acetic acid, 9 mM sorbic acid, or 13 mM benzoic acid (unless otherwise stated, pH of the medium was performed at 6.0). Plates were incubated at 30°C for the indicated numbers of days. When indicated, plates were also incubated at 16 or 40°C.

cells or *rim101*Δ vs. *ccss*Δ *rim101*Δ cells). In many cases, hypersensitivity to CFW suggests impairment of cell wall integrity (Ram and Klis, 2006); however, *ccss*Δ cells exhibited weak resistance to CFW (Figure 2). In contrast, the sensitivity of *ccss*Δ *slt2*Δ cells to CFW was much greater than that of *slt2*Δ cells (Figure 4C), implying that *ccss*Δ cells have a stronger defect of cell wall integrity in the absence of

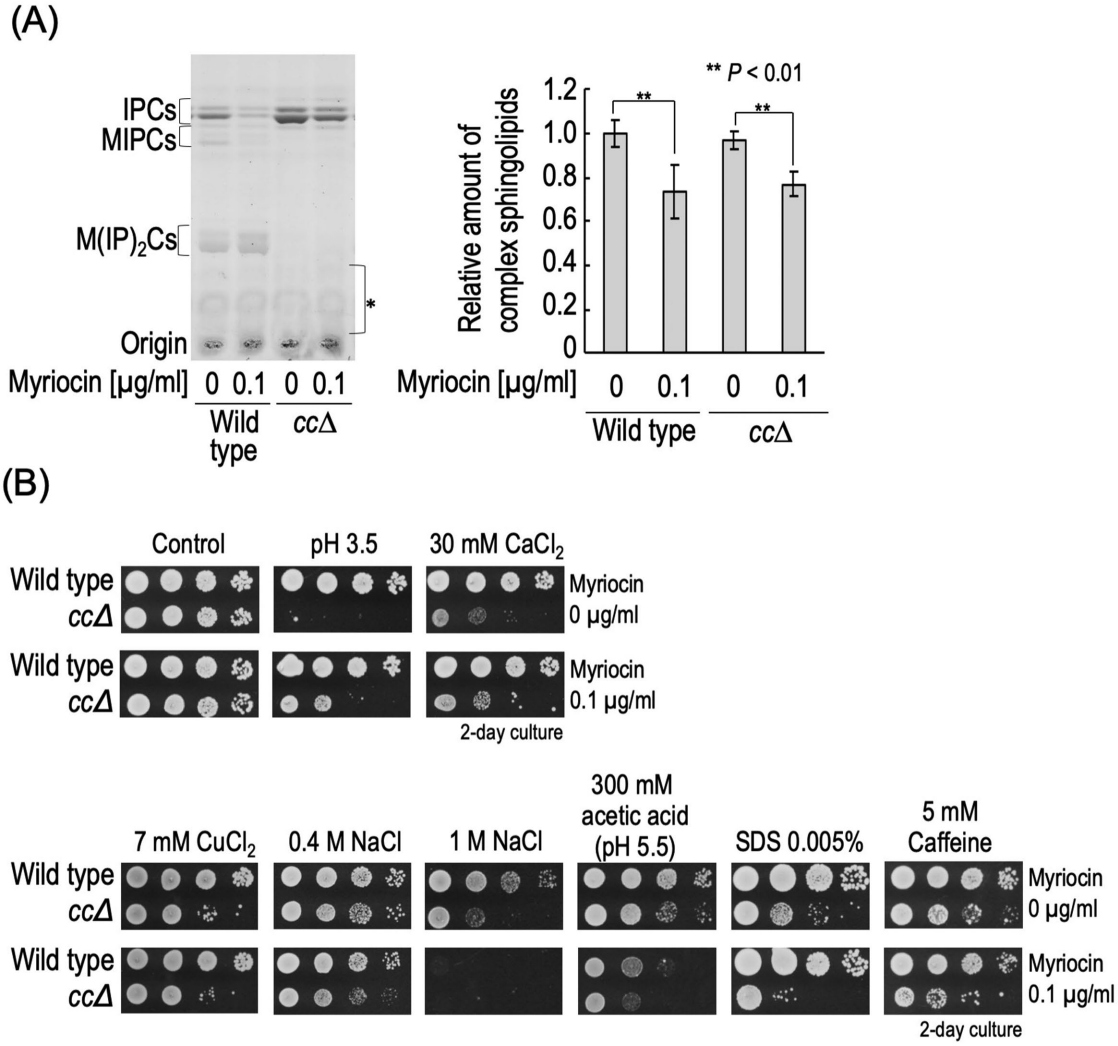

FIGURE 3: Stress sensitivity caused by loss of MIPCs or accumulation of IPCs. (A) Effect of myriocin on complex sphingolipid levels. Cells were cultured overnight in YPD medium at 30°C, diluted (0.3 OD_{600} units/ml) in fresh YPD medium with or without 0.1 μg/ml myriocin, and then incubated for 3 h at 30°C. TLC analysis were performed as described in Figure 1D. The amount of complex sphingolipids (IPCs, MIPCs, and $M(IP)_2Cs$) in myriocin-untreated wild-type cells was taken as 1. (B) Effect of myriocin on sensitivity to stresses. Cells cultured overnight in YPD medium were spotted onto YPD plates containing 30 mM $CaCl_2$, 7 mM $CuCl_2$, 0.4 or 1 M NaCl, 300 mM acetic acid (adjusted to pH 5.5 by the addition of 50 mM MES and MOPS), SDS 0.005%, 5 mM caffeine, or 0.1 μg/ml myriocin, and then incubated for 2 d. YPD plates (pH 3.5) were prepared by the addition of 100 mM Gly-HCl.

SLT2. Similar results were obtained for *cc*Δ cells (Figure 4C) (Morimoto and Tani, 2015). Notably, in the absence of Hog1, Slt2, or Rim101, the enhancing effects of stress sensitivities caused by *ccss*Δ were much more robust than that in the case of *cc*Δ or *ss*Δ (Figure 4, A–C). Next, we examined activation of these signaling pathways in wild-type and *ccss*Δ cells. As shown in Figure 4D, enhancement of phosphorylation of Hog1 in the presence of NaCl was observed in *ccss*Δ cells, although the degree of the increase was lower than that in wild-type cells. However, it is unlikely that the decrease in activation of the HOG pathway causes the hypersensitivity to NaCl in *ccss*Δ cells because salt/hyperosmotic stress hypersensitivity due to *ccss*Δ is observed even in the absence of *HOG1* (Figure 4A). In *ccss*Δ cells, the level of phosphorylated Slt2-6xHA in both the presence and absence of CFW was higher than that in wild-type cells (Figure 4E), suggesting weak constitutive activation of Slt2 due to *ccss*Δ even in the absence of stress. Similar results were obtained when Slt2 was not tagged with 6xHA (unpublished data). It should be noted that the total expression level of Slt2-6xHA in *ccss*Δ cells was also higher than that in wild-type cells regardless of the presence or absence of CFW (Figure 4E). These increases were consistent with the previous finding for *cc*Δ cells (Morimoto and Tani, 2015; Tanaka and Tani, 2018). The increased activity of Slt2 may be the reason why *ccss*Δ cells exhibited CFW resistance as compared with wild-type cells (Figure 2) because *csss*Δ *slt2*Δ cells were more sensitive to CFW than wild-type and *slt2*Δ cells (Figure 4C). A significant difference in nuclear translocation of yeGFP-Rim101 due to alkalinization of the medium was not observed between wild-type and *ccss*Δ cells (Figure 4F). Collectively, these results suggested that the hypersensitivity of *ccss*Δ cells to these stresses is not due to impairment of these stress response systems.

Transcriptional regulation via Msn2 and Msn4 is also involved in the adaptation of cells to various environmental changes, which is known as a "general stress response" (Schmitt and McEntee, 1996; Moskvina *et al*., 1998; Gasch *et al*., 2000). Thus, we also examined

the effect of deletion of *MSN2/4* in *ccss*Δ cells. Deletion of *MSN2/4* caused reduced heat stability (wild-type vs. *msn2/4*Δ cells) (Figure 4G), a typical phenotype of *msn2/4*Δ cells (Wei *et al.*, 2008). *ccss*Δ cells exhibited a slight decrease in heat stability as compared with wild-type cells, and this decrease was more pronounced in the absence of *MSN2/4* (*msn2/4*Δ vs. *ccss*Δ *msn2/4*Δ cells) (Figure 4G). In *ccss*Δ cells, basal transcriptional activity mediated by Msn2/4 was lower than that in wild-type cells but much higher than that in *msn2/4*Δ cells, when estimated using a reporter gene plasmid that contained the α-galactosidase gene and six tandem repeats of the stress response element (STRE), a binding site of Msn2/4 (Martinez-Arias *et al.*, 1984; Schmitt and McEntee, 1996) (Figure 4H). Similar results were obtained when cells were exposed to heat shock (47 or 48°C for 60 min) (Supplemental Figure S5). These results suggested that Msn2/4 is still functional even with mutation of *ccss*Δ.

Slt2 and Msn2/4 are important for maintenance of the growth rate and stress tolerance in *ccss*Δ cells

During evaluation of the stress sensitivities of stress response systems–deleted cells, we noticed that the deletion of *SLT2* or *MSN2/4* dramatically reduced the growth rate of *ccss*Δ cells under normal growth conditions (YPD medium) (Figure 5A and Supplemental Figure S6A), while the deletion of *HOG1* or *RIM101* had only a mild effect (Figure 5A). Although Msn2 and Msn4 are largely, that is, not completely, functionally redundant (Schmitt and McEntee, 1996; Yamaguchi *et al.*, 2018), a single deletion of *MSN2* or *MSN4* does not cause reduction of the growth rate of *ccss*Δ cells (Supplemental Figure S6B), indicating that both Msn2 and Msn4 are required for maintenance of the growth rate of *ccss*Δ cells. The effect of deletion of *SLT2* or *MSN2/4* on the cell growth rate was not severe for *ss*Δ and *cc*Δ cells (Figure 5B). Significant differences in the complex sphingolipid levels between *ccss*Δ and *ccss*Δ *slt2*Δ or *ccss*Δ *msn2/4*Δ cells were not observed (Figure 5C), indicating that the slow growth phenotype due to the deletion of *SLT2* or *MSN2/4* is not caused by reduction of the complex sphingolipid levels. The deletion of *MSN2/4* enhanced the sensitivity of *ccss*Δ cells to pH 8.0, NaCl, sorbitol, acetic acid, and SDS (*ccss*Δ vs. *ccss*Δ *msn2/4*Δ cells) (Figure 5D). Notably, a marked difference was not observed between wild-type and *msn2/4*Δ cells under the experimental conditions used in this study (Figure 5D), indicating that Msn2/4 are involved in compensation for reduced tolerance to these stress conditions due to *ccss*Δ. In contrast, the deletion of *SLT2* did not enhance the hypersensitivity to NaCl, sorbitol, or acetic acid due to *ccss*Δ (Figure 5E). As reported previously (Imazu and Sakurai, 2005), *slt2*Δ cells exhibited hypersensitivity to 40°C, probably because of a defect of the response to cell wall damage due to elevated temperature. Notably, *ccss*Δ *slt2*Δ cells showed very strong sensitivity to 40°C compared with *ccss*Δ and *slt2*Δ cells (Figure 5E); however, *ccss*Δ *msn2/4*Δ cells exhibited sensitivity similar to that of *ccss*Δ cells (Figure 5D). Although *ccss*Δ *slt2*Δ cells were more sensitive to pH 8.0 than *ccss*Δ cells, the sensitivity of *slt2*Δ cells was more severe than that of *ccss*Δ and *ccss*Δ *slt2*Δ cells (Figure 5E). Thus, it was suggested that the deletion of *SLT2* does not contribute to compensation for the pH 8.0 hypersensitivity due to *ccss*Δ. Collectively, these results suggested that both Msn2/4 and Slt2 contribute to compensation for the multiplestress hypersensitivity due to *ccss*Δ; however, their roles are distinctly different.

Notably, deletion of *MSN2/4* increased the hypersensitivity to SDS due to *ccss*Δ, whereas that of *SLT2* suppressed the hypersensitivity (Figure 5, D and E). Deletion of *BCK1* encoding MAPKKK that functions upstream of Slt2 also suppressed the SDS hypersensitivity of *ccss*Δ and *cc*Δ cells (*ccss*Δ vs. *ccss*Δ *bck1*Δ cells or *cc*Δ vs. *cc*Δ *bck1*Δ cells) (Figure 5F). Deletion of *ROM2* encoding a guanine nucleotide exchange factor for Rho1, an upstream factor of the CWI pathway, suppressed the SDS hypersensitivity of *cc*Δ cells (*cc*Δ vs. *cc*Δ *rom2*Δ cells), but did not have such an effect on *ccss*Δ cells (*ccss*Δ vs. *ccss*Δ *rom2*Δ cells) (Figure 5F). This is probably because Rho1 is an essential GTP-binding protein, and thus the deletion of *ROM2* may affect the growth of *ccss*Δ cells by factor(s) other than the defect of the CWI pathway. SDS treatment enhances phosphorylation of Slt2 (Sakata *et al.*, 2022). As shown in Figure 5G, an increase in the level of phosphorylated Slt2-6xHA by the SDS treatment was observed in both wild-type and *ccss*Δ cells, suggesting that the activation of the CWI pathway by SDS also occurs in *ccss*Δ cells. In addition, in both wild-type and *ccss*Δ cells, promoter activity of *NCW2*, one of the downstream targets of Slt2 (this will be described later), was increased by the SDS treatment (Figure 5H). SDS is recognized as a reagent for evaluation of the integrities of both plasma membranes and cell walls; that is, the detrimental effects of SDS are caused by perturbation of the integrity of the cell membrane (Kono *et al.*, 2016; Zhao *et al.*, 2020), and defects of cell wall also lead to increased sensitivity to SDS because a weakened cell wall allows an increase in the accessibility of SDS on plasma membranes (Levin, 2005; Kono *et al.*, 2016; Zhao *et al.*, 2020). Thus, the fact that the defect of the CWI pathway confers resistance to SDS in *ccss*Δ cells probably reflects the impaired integrity of plasma membranes but not cell walls (this will be discussed later).

Cell wall–related genes are abundant among genes whose expression is changed by *ccss*Δ

To investigate how loss of structural diversity of complex sphingolipids affects the gene expression profile, we performed transcriptome analysis by RNA-sequencing for wild-type and *ccss*Δ cells (Figure 6A). It was found that expression of 161 and 160 genes was significantly up-regulated and down-regulated in *ccss*Δ cells, respectively (Figure 6A and Supplemental Table S1). Gene ontology (GO) enrichment analysis of biological processes revealed that genes annotated as "cell wall organization or biogenesis (GO:0071554)" were the most abundant among the genes up-regulated in the *ccss*Δ cells, indicating that cell wall–related genes were predominantly up-regulated in *ccss*Δ cells (Figure 6B). It should be noted that nine genes (*YGP1, NCW2, CRH1, PST1, SED1, KRE6, YPK2, CWP1*, and *HSP150*) annotated as "cell wall organization or biogenesis" were listed in the *Saccharomyces* Genome Database (SGD) (https://www.yeastgenome.org/) as putative downstream targets of Rlm1 and/or Swi4, transcriptional factors of the CWI pathway (Figure 6A), which may be related to the constitutive activation of Slt2 MAP kinase in *ccss*Δ cells (Figure 4E). Thus, we next examined the promoter activity of *NCW2* (target of Swi4), *SED1* (target of Rlm1), and *CRH1* (target of Rlm1 and Swi4) in wild-type, *slt2*Δ, *ccss*Δ, and *ccss*Δ *slt2*Δ cells by using reporter gene plasmids that contain the α-galactosidase gene and a potential promoter region of each gene. As shown in Figure 6D, an increase in these promoter activities was observed in *ccss*Δ cells as compared with wild-type cells. In both wild-type and *ccss*Δ cells, the deletion of *SLT2* slightly but significantly decreased the promoter activity of *NCW2* and *SED1* (wild-type vs. *slt2*Δ cells or *ccss*Δ vs. *ccss*Δ *slt2*Δ cells); however, the deletion did not have such an effect on the promoter activity of *CRH1* in *ccss*Δ cells. Moreover, these promoter activities in *ccss*Δ *slt2*Δ cells were greater than that in *slt2*Δ cells (Figure 6D). These results suggested that the up-regulation of these genes in *ccss*Δ cells at least partly depends on the CWI pathway, but another factor(s) is also involved. In contrast, most of the genes that are listed in the SGD as putative downstream targets of Msn2/4 were not up-regulated in *ccss*Δ cells (Figure 6C),

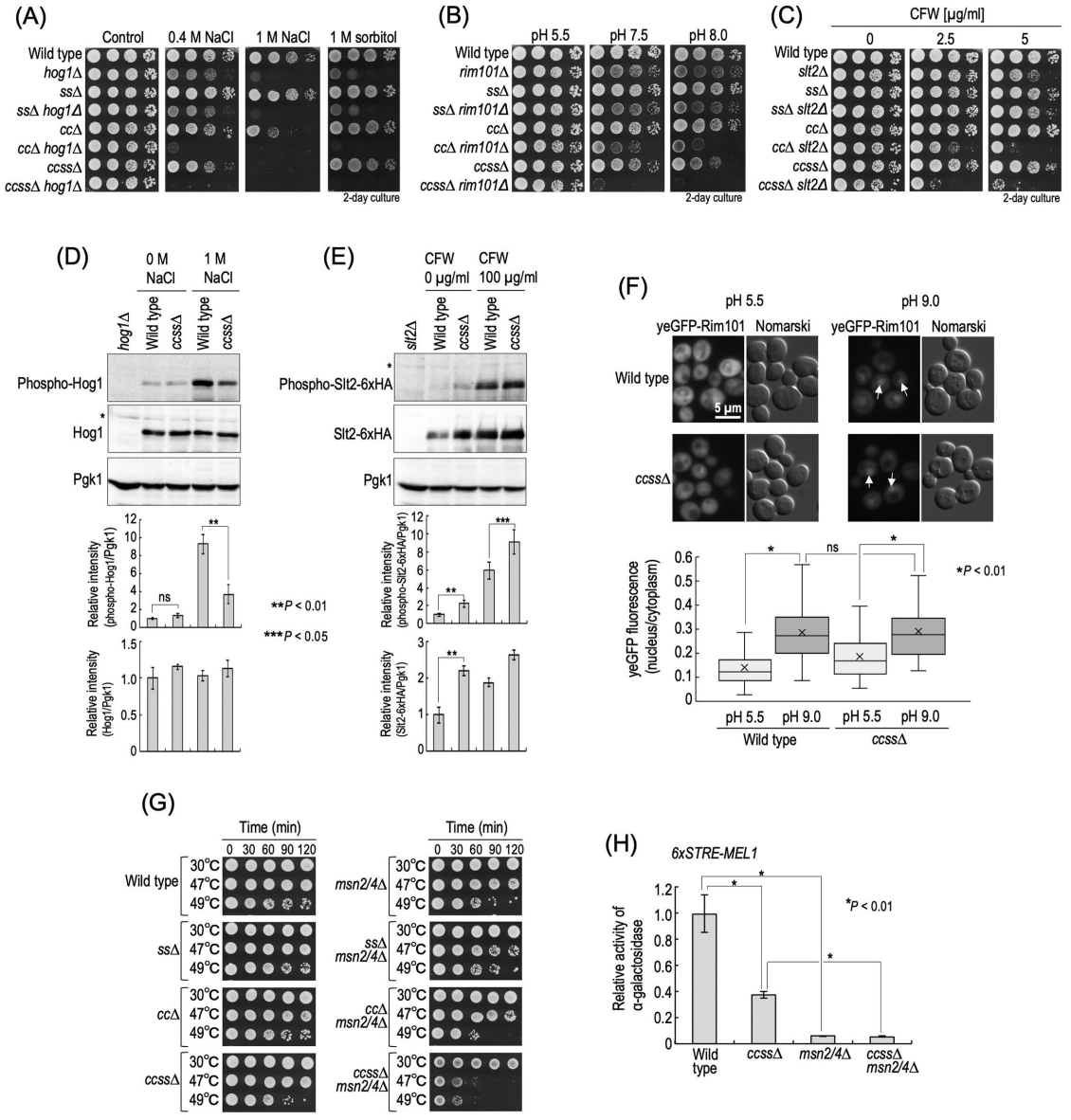

FIGURE 4: Relationship between stress sensitivity of complex sphingolipid diversity–disrupted mutants and stress response systems. (A–C) Cells cultured overnight in YPD medium at 30°C were spotted onto YPD plates containing 0.4 or 1 M NaCl, 2 M sorbitol (A) or 2.5 or 5 μg/ml CFW (C) and then incubated for 2 d. Buffered YPD plates were prepared by the addition of 50 mM MES and MOPS (for pH 5.5) or 100 mM HEPES (for pH 7.5 and 8.0) (B). (D) Western blotting analysis of phosphorylation of Hog1. Cells were cultured overnight in YPD medium, diluted (0.1 OD_{600} units/ml) in fresh YPD medium, and then incubated for 5 h at 30°C. Then, cells were treated with 1 M NaCl (final concentration) for 20 min by the addition of fresh YPD containing 5 M NaCl to the culture medium. For the control experiment (0 M NaCl), an equal volume of fresh YPD medium was added to the culture medium. Yeast cell extracts were immunoblotted using anti–phospho-p38 MAPK (recognizes phospho-Hog1), anti-Hog1, or anti-Pgk1. The relative amount of phospho-Hog1/Pgk1 or phospho-Hog1/Hog1 in wild-type cells without NaCl was taken as 1. (E) Western blotting analysis of phosphorylation of Slt2-6xHA. Cells expressing Slt2-6xHA were precultured as described in D. Then, cells were treated with 100 μg/ml CFW for 30 min. Yeast cell extracts were immunoblotted using anti–phospho-p44/42 MAPK (recognizes phospho-Slt2-6xHA), anti-HA, or anti-Pgk1. The relative amount of phospho-Slt2-6xHA/Pgk1 or Slt2-6xHA/Pgk1 in wild-type cells without CFW was taken as 1. Data represent means ± SD for one experiment (triplicate) representative of three independent experiments. The asterisk indicates unidentified bands. (F) Translocation of yeGFP-Rim101. Cells expressing yeGFP-Rim101 were cultured overnight in YPD medium, diluted (0.1 OD_{600} units/ml) in fresh YPD medium, and then incubated for 4 h at 30°C. For alkaline treatment to activate the Rim101 pathway, Tris-HCl (pH 9.0) was added to the culture medium at a final concentration of 100 mM. For the control experiment, MES and MOPS (pH 5.5) were added at a final concentration of 50 mM. Cells were incubated for 60 min at 30°C, fixed, and then viewed under a fluorescence microscope. The arrows indicate nuclear localization of yeGFP-Rim101. The ratio of yeGFP fluorescence in cytoplasm and the nucleus in individual cells is expressed as a boxplot. Data represent the values for 100 cells for individual strains. (G) Heat stability. Cells (0.7 OD_{600} units) grown in YPD medium were collected by centrifugation, washed with water, and then suspended in 1 ml of water. The cell suspensions were incubated for the indicated times at

which coincided with the results of reporter gene assays (Figure 4H). These results suggested that the expression profile of cell wall–related genes was greatly affected by loss of structural diversity of complex sphingolipids.

Defect of cell wall integrity in *ccssΔ* cells

Transcriptome analysis (Figure 6A) and the effect of deletion of *SLT2* on the sensitivities to CFW and 40°C (Figures 4C and 5E) prompted us to investigate cell wall integrity in *ccssΔ* cells. Thus, we examined the sensitivity to zymolyase, a cell wall–digesting enzyme, for evaluation of the cell wall integrity. As shown in Figure 6E, *ccssΔ* cells were slightly but significantly more sensitive to zymolyase than wild-type cells, suggesting decreased cell wall integrity due to *ccssΔ*. Moreover, deletion of *SLT2* further promoted the increased sensitivity to zymolyase due to *ccssΔ* (Figure 6E), whereas a notable difference was not observed between wild-type and *slt2Δ* cells (Figure 6E and Supplemental Figure S7). Thus, it was indicated that, unlike wild-type cells, *ccssΔ* cells are strongly dependent on maintenance of cell wall integrity by the CWI pathway even in the absence of stresses. This notion is supported by the fact that Slt2 is constitutively activated in *ccssΔ* cells (Figure 4E). Previously, we reported that *ccΔ* cells also exhibit increased sensitivity to zymolyase (Morimoto and Tani, 2015); however, the zymolyase sensitivity of *ccssΔ slt2Δ* cells was greater than that of *ccΔ slt2Δ* cells (Supplemental Figure S7). In addition, *ccssΔ slt2Δ* cells were more sensitive to CFW than *ccΔ slt2Δ* and *ssΔ slt2Δ* cells (Figure 4C). Thus, it was indicated that the additional defect of hydroxylation of the Cer moiety causes a more serious defect of cell wall integrity in MIPC biosynthesis–deficient cells. Interestingly, deletion of *MSN2/4* suppressed the zymolyase hypersensitivity due to *ccssΔ* (Figure 6E). The exact reason for this is unclear, but at least this suggests that Msn2/4 do not contribute to maintenance of cell wall integrity in *ccssΔ* cells.

Maintenance of plasma membrane integrity in *ccssΔ* cells by Msn2/4

Maintenance of integrity of plasma membranes is important for acquirement of tolerance to various stresses (Mioka *et al.*, 2018; Kishimoto *et al.*, 2021). *ccssΔ* cells exhibit abnormal lateral diffusion of membrane proteins at plasma membranes (Uemura *et al.*, 2014), suggesting a change in the properties of plasma membranes due to loss of structural diversity of complex sphingolipids. Thus, it became important to investigate whether or not *ccssΔ* affects the integrity of plasma membranes. To examine this, we evaluated the permeability of plasma membranes by observing the efficiency of incorporation of a lipofilic fluorescent dye, rhodamine 6G, into cells (Mioka *et al.*, 2018). Because incorporated rhodamine 6G is extruded in an ATP-dependent manner (Mioka *et al.*, 2018), the examination of incorporation of the dye was performed under ATP-depleted conditions. Intracellular accumulation of the dye was significantly reduced in *ssΔ* cells (Figure 7, A and B), and a reduction was also observed in *sur2Δ* or *scs7Δ* cells (Figure 7C), indicating that loss of either *SUR2* or *SCS7* causes decreased permeability of plasma membranes. In contrast, notable differences were not observed between wild-type, *ccΔ*, and *ccssΔ* cells; however, *ccssΔ msn2/4Δ* cells exhibited a marked increase in accumulation of the dye (Figure 7, A and B). Such an increase was not observed in *msn2/4Δ*, *ccΔ msn2/4Δ*, and *ssΔ msn2/4Δ* cells (Figure 7B), suggesting that Msn2/4 are involved in suppression of the increase in plasma membrane permeability due to *ccssΔ*. In contrast, the deletion of *SLT2* did not affect the plasma membrane permeability in *ccssΔ* cells (Figure 7, A and B). Deletion of *MSN2/4* further promotes hypersensitivity to NaCl, sorbitol, SDS, acetic acid, and pH 8.0 due to *ccssΔ* (Figure 5D), and thus it is possible that, even in the presence of *MSN2/4*, the permeability of plasma membranes of *ccssΔ* cells changes under these stresses. Therefore, we next investigated the accumulation of rhodamine 6G in wild-type, *ssΔ*, *ccΔ*, and *ccssΔ* cells under these stresses. To eliminate the possibility that depletion of ATP has detrimental effects on cells in the presence of each stress, these experiments were performed under the condition that ATP is not depleted. As show in Figure 7D, similar to the ATP-depleted conditions, a decrease or increase in plasma membrane permeability was observed in *ssΔ* or *ccssΔ msn2/4Δ* cells, respectively, when ATP was not depleted. In the presence of 1 M NaCl, 2 M sorbitol, or 0.005% SDS, the accumulation of rhodamine 6G in *ccssΔ* cells was increased as compared with that in wild-type cells (Figure 7, E–G), whereas the accumulation of the dye in *ccssΔ* cells was not increased in the presence of acetic acid or under pH 8.0 conditions (Figure 7, H and I). Because hyperosmotic stresses cause a change in the tension of plasma membranes due to shrinkage of cells (Dupont *et al.*, 2010; Petelenz-Kurdziel *et al.*, 2011), and SDS directly damages plasma membranes (Kono *et al.*, 2016; Zhao *et al.*, 2020), these results support the notion that the properties of plasma membranes are altered due to *ccssΔ*. These results may also suggest that multiplestress hypersensitivity due to loss of structural diversity of complex sphingolipids is caused, at least partly, by the abnormal plasma membrane property. To gain further insight into the physical properties of plasma membranes, we used di-4-ANEPPDHQ, a probe for evaluating membrane lipid order (Owen *et al.*, 2011). When cells were stained with di-4-ANEPPDHQ for 1 min, most of fluorescence signal was observed at the cell surface (Supplemental Figure S8). di-4-ANEPPDHQ has green fluorescence when residing in the ordered phase of membranes and red fluorescence in the disordered phase (Owen *et al.*, 2011). Figure 7J shows the ratio of green (525 nm) and red (610 nm) fluorescences in each cell, measured by a flow cytometer. *ERG6*-deleted cells, which exhibit increases in both plasma membrane permeability and fluidity (Abe and Hiraki, 2009; Khmelinskaia *et al.*, 2020), showed a decrease in the green/red fluorescence ratio as compared with wild-type cells, suggesting lower lipid order in plasma membranes (Figure 7J). In contrast, *ssΔ* and *ccssΔ* cells exhibited higher lipid order in plasma membranes as compared with wild-type cells (Figure 7J). These results are probably consistent with the fact that speed of lateral diffusion of plasma membrane–localized hexose transporter 1 is decreased due to *ccssΔ* (Uemura *et al.*, 2014). The deletion of *MSN2/4* caused a decrease in the green/red fluorescence ratio in *ccssΔ* cells (*ccssΔ* vs. *ccssΔ msn2/4Δ* cells), whereas no significant difference was observed between wild-type and *msn2/4Δ* cells (Figure 7J). These results suggested that a defect of structural diversity of complex sphingolipids alters physical

the indicated temperatures, and samples (3.5 µl) were spotted onto YPD plates and then incubated for 2 d.
(H) STRE-mediated transcriptional activity. Cells harboring pRS416-*6xSTRE-MEL1* were cultured overnight in SC medium lacking uracil (SC–Ura), diluted (0.3 OD_{600} units/ml) in fresh SC–Ura medium, and then incubated for 6 h at 30°C. Cells were harvested, and α-galactosidase activity was measured. Data represent means ± SD for one experiment (triplicate) representative of three independent experiments. ns: no significant difference. The details are given in *Materials and Methods*.

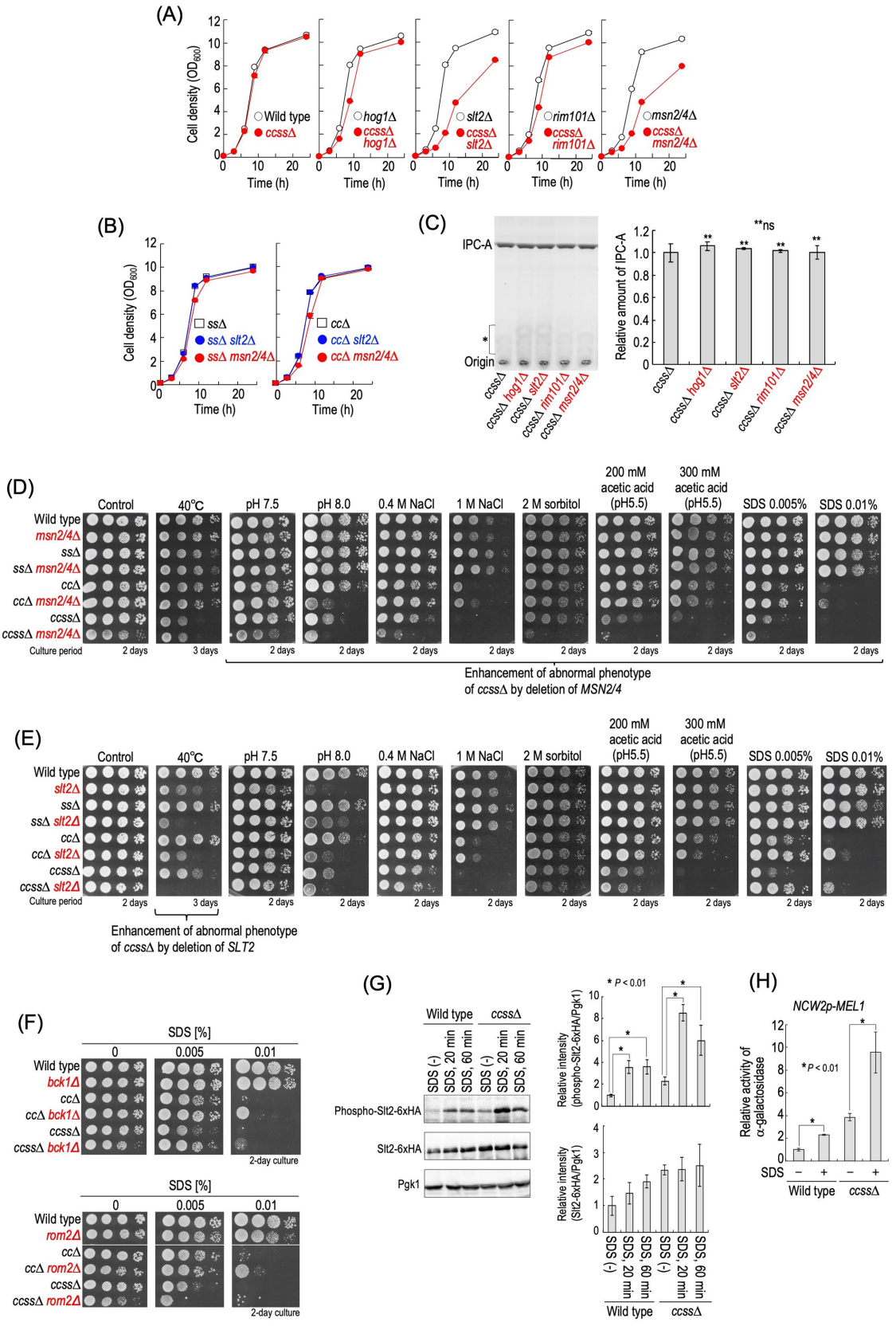

FIGURE 5: Slt2- and Msn2/4-dependent cell growth and stress tolerance of *ccss*Δ cells. (A) Effect of deletion of *HOG1*, *SLT2*, *RIM101*, or *MSN2/4* on cell growth of *ccss*Δ cells. Cells were cultured overnight in YPD medium at 30°C and diluted (0.1 OD_{600} units/ml) in fresh YPD medium, and then aliquots of cell suspensions were subjected to cell density measurements (OD_{600}) at the indicated times. (B) Effect of deletion of *SLT2* or *MSN2/4* on the cell growth of *cc*Δ and *ss*Δ cells. (C) Effect of deletion of *HOG1*, *SLT2*, *RIM101*, or *MSN2/4* on the IPC-A level in *ccss*Δ cells. TLC analysis was

properties of plasma membranes. Eisosomes, which are furrow-like structures at plasma membranes, have important roles in acquirement of stress tolerance (Dupont *et al.*, 2010; Sakata *et al.*, 2022), and several reports suggest functional relationship between eisosomes and sphingolipids (Walther *et al.*, 2007; Luo *et al.*, 2008; Frohlich *et al.*, 2009). However, difference of distribution pattern of eisosomes was not observed between wild-type and *ccss*Δ cells when eisosomes were detected by Pil1-yeGFP, an eisosome marker protein (Walther *et al.*, 2007) (Figure 7K).

Rescue of the integrity of cell walls, but not plasma membranes, in *ccss*Δ cells by sterols

Complex sphingolipids and sterols are known to function coordinately (Guan *et al.*, 2009; Tanaka and Tani, 2018; Otsu *et al.*, 2020). Thus, we next investigated cellular sterol levels in wild-type, *cc*Δ, *ss*Δ, *ccss*Δ, *ipt1*Δ, and *ipt1*Δ *ss*Δ cells. As shown in Figure 8A, *ccss*Δ cells exhibited a significant decrease in the sterol levels as compared with wild-type cells. Moreover, *ccss*Δ cells exhibited decreased sensitivity to the polyene antifungal nystatin (Figure 8B), which exerts cytotoxicity through binding to ergosterol at plasma membranes and subsequently formation of channels (Serhan *et al.*, 2014). When cells were stained with filipin, a fluorescent probe that stains sterols, the fluorescence intensity at plasma membranes in *ccss*Δ cells was decreased as compared with that in wild-type cells, also suggesting a decrease in sterol levels (Figure 8C). To investigate whether or not this decrease is related to hypersensitivity of *ccss*Δ cells to multiplestresses, *SIP3*, *LAM1*, or *YSP2* encoding sterol-transfer protein involved in trafficking of sterols from plasma membranes to the ER (Gatta *et al.*, 2015) was deleted in order to alter the distribution pattern of sterols at plasma membranes. Although *ccss*Δ cells, compared with wild-type cells, exhibited resistance to nystatin, the resistance was suppressed by the deletion of *SIP3*, *LAM1*, or *YSP2* (Figure 8B). Furthermore, when cells were stained with filipin, the deletion of *SIP3*, *LAM1*, or *YSP2* recovered the decrease in the fluorescence intensity due to *ccss*Δ (Figure 8C). These results suggested a change of the distribution pattern of sterols at plasma membranes in *ccss*Δ cells by the deletion of *SIP3*, *LAM1*, or *YSP2*. The deletion of *SIP3*, *LAM1*, or *YSP2* did not suppress the hypersensitivities to NaCl, acetic acid, pH 8.0, and SDS due to *ccss*Δ (Figure 8D). In contrast, these deletions abolished the hypersensitivity to 40°C due to *ccss*Δ (Figure 8D). The hypersensitivities to NaCl, acetic acid, pH 8.0, and SDS due to *ccss*Δ were enhanced by the deletion of *MSN2/4* (Figure 5D), whereas the hypersensitivity to 40°C was enhanced by that of *SLT2* (Figure 5E), which may imply that the deletion of *SIP3*, *LAM1*, or *YSP2* improves the defect of cell wall integrity due to *ccss*Δ. Thus, we next examined the zymolyase sensitivity of *SIP3*-deleted cells. In this experiment, *SLT2* was deleted in all strains in order to allow clear observation of the increase in zymolyase sensitivity due to *ccss*Δ. As shown in Figure 8E, the hypersensitivity to zymolyase in *ccss*Δ *slt2*Δ cells was suppressed by the deletion of *SIP3* (*ccss*Δ *slt2*Δ vs. *ccss*Δ *slt2*Δ *sip3*Δ cells); however, the deletion did not improve the zymolyase sensitivity of *slt2*Δ cells (*slt2*Δ vs. *slt2*Δ *sip3*Δ cells). Thus, it was suggested that alteration of the distribution pattern of sterols at plasma membranes compensates for the impaired cell wall integrity due to *ccss*Δ. In contrast, the increase in accumulation of rhodamine 6G due to *ccss*Δ *msn2/4*Δ was not suppressed by deletion of *SIP3* in either the absence or the presence of ATP (*ccss*Δ *msn2/4*Δ vs. *ccss*Δ *msn2/4*Δ *sip3*Δ cells) (Figure 8, F and G), suggesting that sterols do not improve the impairment of plasma membrane integrity due to *ccss*Δ, which coincided with the fact that the deletion of *SIP3* did not suppress the hypersensitivities to NaCl, acetic acid, pH 8.0, and SDS due to *ccss*Δ (Figure 8D). It should be noted that the deletion of *MSN2*/4 did not enhance the reduction in the sterol levels due to *ccss*Δ (Supplemental Figure S9), supporting the notion that sterols are not involved in compensation for the impaired integrity of plasma membranes due to *ccss*Δ. Moreover, the deletion of *SLT2* also did not affect the sterol levels in *ccss*Δ cells (Supplemental Figure S9), indicating that increased impairment of cell wall integrity in *ccss*Δ *slt2*Δ cells is not caused by enhancement of the decrease in the sterol levels.

DISCUSSION

In this study, we created a complex sphingolipid structural diversity disruption library and evaluated various environmental stress sensitivities of the library mutants. As a general tendency, it was found that the more the structural variation of complex sphingolipids is limited, the more stress sensitivity tends to increase (Figure 2). In particular, in many cases, loss of MIPC biosynthesis (*cc*Δ) triggers the occurrence of stress hypersensitivity, and the detrimental effects were promoted by the loss of hydroxylation of the Cer moiety (*sur2*Δ, *scs7*Δ, or *ss*Δ) (Figure 2). Moreover, it was suggested that these abnormal phenotypes, except for hypersensitivities to low pH and $CaCl_2$, are caused by loss of production of MIPCs, but not by accumulation of IPCs (Figure 3 and Supplemental Figure S3). Thus, these results imply that, among complex sphingolipid subtypes, MIPCs are the most important factor for the acquirement of stress tolerance in budding yeast. Loss of MIPC biosynthesis causes loss of $M(IP)_2Cs$ as well as MIPCs; however, loss of $M(IP)_2C$ biosynthesis (*ipt1*Δ) hardly affected the stress sensitivities, suggesting the importance of MIPCs but not $M(IP)_2Cs$. However, it should be noted that it was not possible to establish a mutant in which $M(IP)_2Cs$ are produced but MIPCs are not produced (Figure 1D). Furthermore, MIPCs were accumulated, as compared with in wild-type cells, in *IPT1*-deleted cells (Figure 1D). Thus, it is not possible to conclude whether

performed as described in Figure 1, D and E. Data represent means ± SD for one experiment (triplicate) representative of three independent experiments. ns: no significant difference. (D, E) Effects of deletion of *MSN2/4* (D) or *SLT2* (E) on stress sensitivities. Cells cultured overnight in YPD medium were spotted onto YPD plates (the details of the composition of the medium are given in Figure 2). Plates were incubated at 30 or 40°C for the indicated numbers of days. (F) Effects of deletion of *BCK1* or *ROM2* on SDS sensitivity. (G) Phosphorylation of Slt2-6xHA in SDS-treated cells. Cells expressing Slt2-6xHA were cultured overnight in YPD medium, diluted (0.3 OD_{600} units/ml) in fresh YPD medium, incubated for 5 h at 30°C, and then treated with 0.01% SDS for 20 or 60 min. Yeast cell extracts were immunoblotted using anti–phospho-p44/42 MAPK, anti-HA, or anti-Pgk1. The relative amount of phospho-Slt2-6xHA/Pgk1 or Slt2-6xHA/Pgk1 in SDS-untreated wild-type cells was taken as 1. (H) Promoter activity of *NCW1* in SDS-treated cells. Cells harboring pRS415-*NCW2p-MEL1* were cultured overnight in SC–Leu medium, diluted (0.3 OD_{600} units/ml) in fresh SC–Leu medium, and then incubated for 5 h at 30°C. Cells were treated with or without 0.01% SDS for 60 min and harvested, and then α-galactosidase activity was measured. The activity in wild-type cells without SDS was taken as 1. Data represent means ± SD for one experiment (triplicate) representative of three independent experiments. The details are given in *Materials and Methods*.

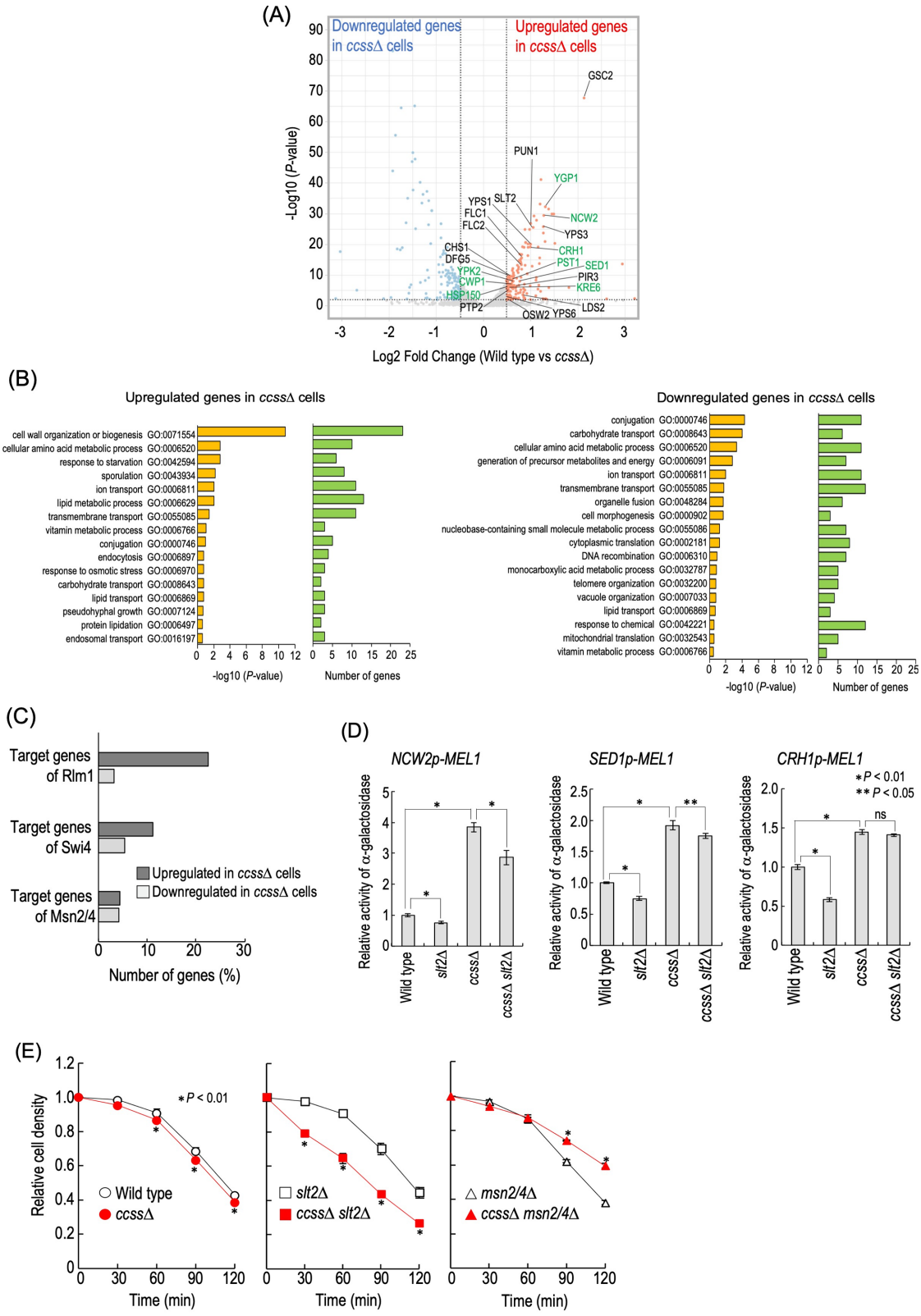

FIGURE 6: Cell wall–related phenotypes of *ccss*Δ cells. (A) Volcano plot for comparison of RNA-sequencing data between wild-type and *ccss*Δ cells. Up-regulated and down-regulated genes due to *ccss*Δ (*P* value ≤ 0.01 and fold change ≥1.4) are denoted in red and blue, respectively. Among up-regulated genes in *ccss*Δ cells, genes annotated as "cell wall organization or biogenesis (GO:0071554)" are marked (23 genes). In addition, of these genes, the genes listed as putative downstream targets of Rlm1 and/or Swi4 (transcriptional factors of the CWI pathway) in the *Saccharomyces* Genome Database (SGD) (https://www.yeastgenome.org/) are in green. (B) Gene ontology (GO) enrichment analysis. GO (biological process) enrichment analysis of up-regulated or down-regulated genes due to *ccss*Δ was performed

the occurrence of the stress hypersensitivities due to *cc*Δ is caused by the disappearance of MIPCs alone or by the disappearance of both MIPCs and $M(IP)_2Cs$. *ccss*Δ cells, which were the most severely sensitive to many stresses, exhibited an increase in permeability of plasma membranes and enhancement of impairment of cell wall integrity upon deletion of *MSN2/4* and *SLT2,* respectively, both of which may affect the acquirement of tolerance of multiple stresses in *ccss*Δ cells (Figures 6E, 7, and 5, D and E). In contrast, the detrimental effects of the deletion of *MSN2/4* or *SLT2* on wild-type cells were mild or hardly detectable (Figures 5, 6E, and 7B), indicating that *ccss*Δ cells are more dependent on Msn2/4 and Slt2 than wild-type cells. It should be noted that there are hundreds of target genes in Msn2/4, and thus it is unclear whether the detrimental effects of the deletion of *MSN2/4* on *ccss*Δ cells can be explained only by the impairment of plasma membrane integrity.

Previously, it was found that the HOG pathway is activated on repression of IPC synthase or SPT, which causes reduction in total levels of complex sphingolipids, and the activation is required for maintenance of cell growth under complex sphingolipid biosynthesis–defective conditions (Tanigawa *et al.*, 2012; Yamaguchi *et al.*, 2018). In contrast, the phosphorylation of Hog1 was not enhanced by *ccss*Δ (Figure 4D), and the deletion of *HOG1* had only a mild effect on the growth of *ccss*Δ cells as compared with that of IPC synthase- or SPT-repressed cells (Figure 5A) (Yamaguchi *et al.*, 2018). Because the total amount of complex sphingolipids was not decreased in *ccss*Δ cells (Figure 1E), it is suggested that the HOG pathway is activated through reduction of the total amount of complex sphingolipids, but not through a defect of structural diversity of complex sphingolipids. These results also suggest that the activation of the HOG pathway is not necessarily required for compensation for the defect of structural diversity of complex sphingolipid due to *ccss*Δ. Msn2/4 are activated by Hog1 and involved in the rescue effect of the HOG pathway under complex sphingolipid biosynthesis–defective conditions (Yamaguchi *et al.*, 2018; Urita *et al.*, 2022). Msn2/4 are involved in the maintenance of plasma membrane integrity and acquirement of tolerance of several stresses in *ccss*Δ cells, whereas the Msn2/4-mediated transcriptional activity was decreased rather than increased in *ccss*Δ cells (Figure 4H). Moreover, in *ccss*Δ cells, overexpression of *MSN2*, which suppresses the growth defect due to reduction of the total amount of complex sphingolipids (Yamaguchi *et al.*, 2018) (Supplemental Figure S10A), did not confer marked resistance to stresses whose sensitivity was enhanced by the deletion of *MSN2/4* (Supplemental Figure S10B and Figure 5D). Thus, it was suggested that, in *ccss*Δ cells, activation of Msn2/4 is not necessarily required as well as the HOG pathway; however, the basal activity of Msn2/4 is necessary and sufficient for the protective effects.

How does *ccss*Δ cause abnormality in plasma membrane properties? Through in silico analysis, Lindahl *et al.* (2016) suggested that a decrease in the ratio of complex sphingolipids in membranes causes a decrease in thickness and density of the lipid bilayer. In addition, it was also proposed that the formation of hydrogen bonds between complex sphingolipid molecules via the hydroxy group of the Cer moiety contributes to stabilization of membranes (Slotte, 2016). These results suggest that complex sphingolipids and their hydroxylation state are important for the maintenance of membrane integrity. However, in *ss*Δ cells, the permeability of plasma membranes was decreased rather than increased (Figure 7, A–C). Furthermore, lateral diffusion of plasma membrane–localized hexose transporter 1 is decreased due to *ccss*Δ, which may imply decreased fluidity of plasma membranes (Uemura *et al.*, 2014). In addition, lipid order in plasma membranes of *ss*Δ and *ccss*Δ cells, which was evaluated by di-4-ANEPPDHQ, was higher than that of wild-type cells (Figure 7J). Thus, it is assumed that the abnormal plasma membrane properties due to the defect of structural diversity of complex sphingolipids is caused by complex factors. One possible explanation is that the defect of the structural diversity may result in alteration of the complex sphingolipid subcellular distribution, including in plasma membranes. It was reported that, in wild-type cells, the distribution pattern of complex sphingolipids depends on their structure; that is, MIPCs and $M(IP)_2Cs$ are relatively abundant in plasma membranes, whereas IPCs are also abundantly detected in the Golgi apparatus and vacuoles, other than plasma membranes (Hechtberger *et al.*, 1994). In addition, the deletion of *SUR2* causes loss of production of phytosphingosine from dihydrosphingosine, both of which function as molecules regulating various signal transduction systems (Chung *et al.*, 2001; Pina *et al.*, 2018; Yabuki *et al.*, 2019; Arita *et al.*, 2020). Furthermore, deletion of either or both *SCS7* and *SUR2* also results in structural changes in free Cer, a precursor of complex sphingolipids (Haak *et al.*, 1997). In most cases, the deletion of *SUR2, SCS7*, or both did not cause stress hypersensitivity unless there was an additional deletion of *CSG1* and *CSH1* (Figure 2), and the intracellular amounts of free LCBs and Cers are much lower than that of complex sphingolipids in the steady state (Ejsing *et al.*, 2009); however, it may also be necessary to consider the effect of structural alteration of free LCBs and Cers on plasma membrane properties.

When plasma membrane stress occurs due to an increase in the tension of membranes, the target of rapamycin complex 2(TORC2)/Ypk1 pathway is activated and subsequently increases the sphingolipid levels for a stress response (Roelants *et al.*, 2017). Furthermore, the phosphorylation of Ypk1 by TORC2 is also increased on deletion of *CSG2* or *CSG1* (Berchtold *et al.*, 2012), which may suggest that abnormalities in plasma membrane properties caused by these mutations are alleviated by the TORC2/Ypk1 pathway. Thus, it is

using the Gene Ontology Slim Term Mapper in the SGD (https://www.yeastgenome.org/goSlimMapper). GO terms significantly enriched in the up-regulated or down-regulated genes (–log10[*P* value] ≥ 0.5) are shown. The enrichment *P* values were calculated using Fisher's exact test. (C) Percentages of numbers of genes up-regulated or down-regulated in *ccss*Δ cells among the putative target genes of Rlm1, Swi4, or Msn2/4 listed in the SGD. (D) Promoter activities of *NCW1*, *SED1*, and *CRH1*. Cells harboring pRS415-*NCW2p-MEL1,* pRS415-*SED1p-MEL1,* or pRS415-*CRH1p-MEL1* were cultured overnight in SC–Leu medium, diluted (0.5 OD_{600} units/ml) in fresh SC–Leu medium, and then incubated for 5 h at 30°C. Cells were harvested, and then α-galactosidase activity was measured. The activity in wild-type cells was taken as 1. Data represent means ± SD for one experiment (triplicate) representative of three independent experiments. ns: no significant difference. (E) Zymolyase sensitivity. Cells were cultured overnight in YPD medium at 30°C, diluted (0.3 OD_{600} units/ml) in fresh YPD medium, and then incubated for 5 h at 30°C. They were then washed with 20 mM HEPES buffer (pH 7.5), resuspended (1.5 OD_{600} units/ml) in the same buffer containing 15 μg/ml zymolyase-20T (Nacalai Tesque), and incubated at 30°C. At the indicated times, the cell density (OD_{600}) in the cell suspensions was measured. Data represent means ± SD for one experiment (triplicate) representative of three independent experiments. The details are given in *Materials and Methods*.

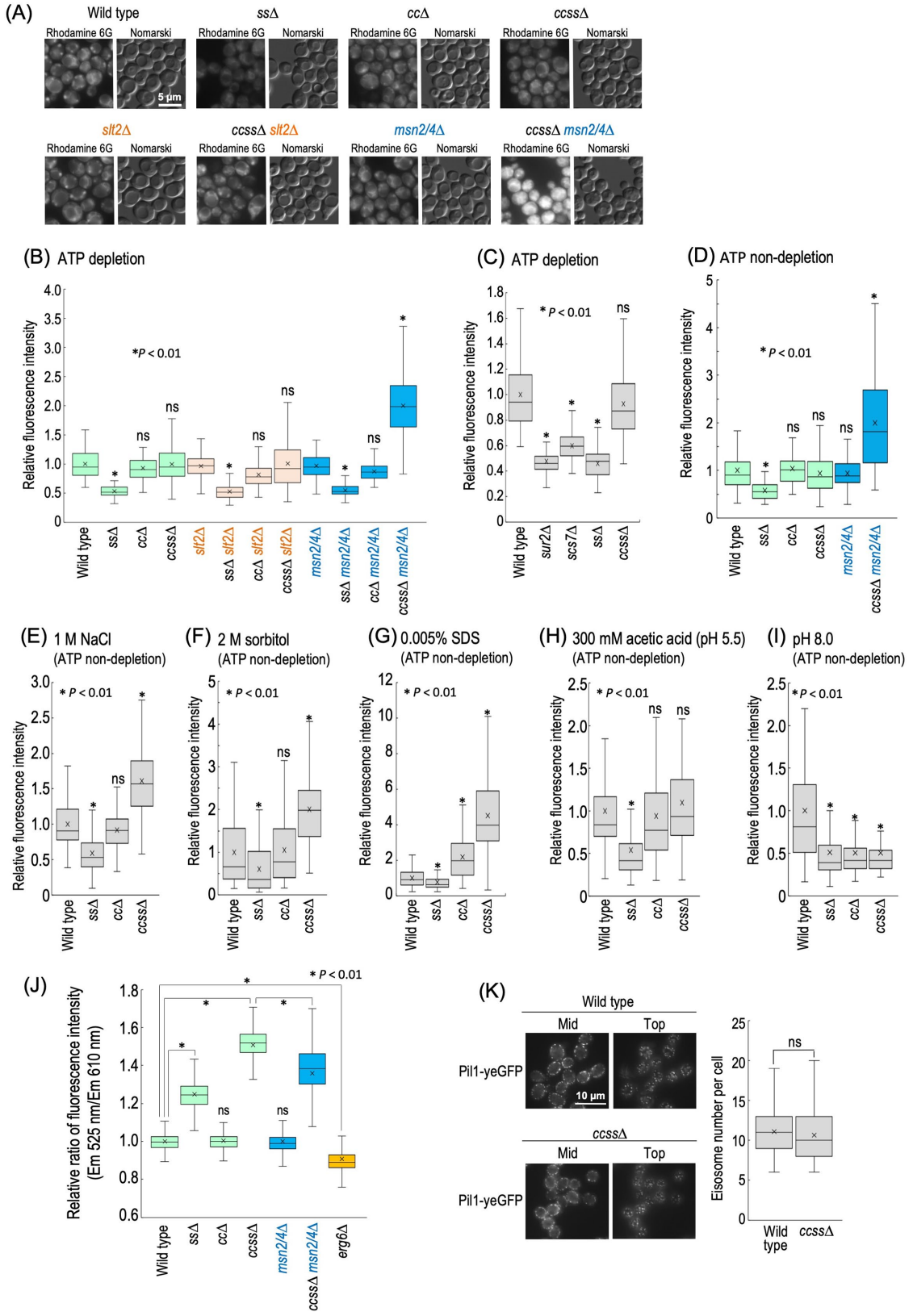

FIGURE 7: Plasma membrane properties in *ccss*Δ cells. (A) Detection of rhodamine 6G incorporated into cells under ATP-depleted conditions. Cells were cultured overnight in YPD medium at 30°C, diluted (0.3 OD_{600} units/ml) in fresh YPD medium, and then incubated for 5 h at 30°C. Rhodamine 6G (10 μM) was added to cells (1 OD_{600} units/300 μl) under ATP-depleted conditions, followed by incubation for 30 min at 30°C. Cells were viewed under a fluorescence microscope. (B, C) Efficiency of incorporation of rhodamine 6G into cells under ATP-depleted conditions. The fluorescence intensity of individual cells is expressed as a boxplot. Data represent the value for 100 cells for individual strains. The average (marked as x) of fluorescence intensity in wild-type cells was taken as 1. ns: no significant

possible that the slow growth phenotype and increases in stress sensitivities of *ccssΔ msn2/4Δ* cells are caused by disturbance of the TORC2/Ypk1 pathway due to the deletion of *MSN2/4*. However, the level of IPC-A in *ccssΔ msn2/4Δ* cells was not decreased as compared with that in *ccssΔ* cells (Figure 5C), suggesting that the TORC2/Ypk1 pathway is not involved in the abnormal phenotypes due to the deletion of *MSN2/4*. This also suggests that Msn2/4 are involved in the rescue of abnormal phenotypes due to *ccssΔ* by affecting other functions rather than regulation of complex sphingolipid biosynthesis. This notion also applies to Slt2, because the deletion of *SLT2* also did not cause a decrease in the IPC-A level in *ccssΔ* cells (Figure 5C). However, it should also be considered the fact that the activation of Slt2 downregulates the activity of TORC2, which may suggest the connection between Slt2 and the TORC2/Ypk1 pathway in *ccssΔ* cells (Leskoske *et al*., 2018).

In summary, the present study indicated a relationship between the structural diversity of complex sphingolipids and tolerance to various environmental stresses and compensation mechanisms against the defect of structural diversity. To further investigate the relationship between complex sphingolipids and stress tolerance, it will be necessary to pursue mechanisms that protect themselves by actively altering the composition of complex sphingolipids in the presence of various stresses. For example, it was reported that spontaneous alteration of the composition of complex sphingolipids is required for adaptation of yeast cells to extracellular low pH conditions and impairment of intracellular H^+ homeostasis due to a defect of vacuolar H^+-ATPase (Tani and Toume, 2015; Otsu *et al*., 2020). Elucidation of such mechanisms will provide deeper insights into the physiological significance of the structural diversity of complex sphingolipids.

MATERIALS AND METHODS

Request a protocol through *Bio-protocol*.

Yeast strains and media

The *S. cerevisiae* strains used are listed in Table 1, and the methods used for genetic modification of yeast strains and construction of plasmids are described in the Supplemental Materials and Methods. The cells were cultured in YPD medium (1% yeast extract, 2% peptone, and 2% glucose [pH 6.0]) or SC (synthetic complete) medium (0.67% yeast nitrogen base without amino acids [BD Difco, Heidelberg, Germany] and 2% glucose [pH 6.0]) containing nutritional supplements. Buffered medium was prepared by the addition of 100 mM glycine-HCl (for pH 3.5), 50 mM MES, and 50 mM MOPS (for pH 5.5), or 100 mM HEPES (for pH 7.5 and 8.0).

Spot assays

Cells were cultured overnight in YPD medium at 30°C and then spotted onto YPD plates in 10-fold serial dilutions starting with a density of 0.7 OD_{600} units/ml. All plates were incubated at 30°C and photographed after 1–3 d. When indicated, plates were also incubated at 16 or 40°C.

Lipid extraction and TLC analysis

Lipids were extracted from *S. cerevisiae* as described previously (Hanson and Lester, 1980) with minor modifications. Briefly, cells (3 OD_{600} units [for detection of complex sphingolipids] or 1.5 OD_{600} units [for detection of sterols]) were suspended in 350 µl of ethanol/water/diethyl ether/pyridine/15 M ammonia (15:15:5:1:0.018, vol/vol) and then incubated at 65°C for 15 min. The lipid extract was centrifuged at 10,000 × *g* for 1 min and then extracted once more in the same manner. The resulting supernatants were dried. For analysis of complex sphingolipids but not sterols, the lipid extracts were dissolved in 130 µl of monomethylamine (40% methanol solution)/water (10:3, vol/vol), incubated for 1 h at 53°C (mild alkaline treatment), and then dried. The lipids were suspended in 60 µl of chloroform/methanol/water (5:4:1, vol/vol), and then separated on Silica Gel 60 TLC (thin-layer chromatography) plates (Merck, Whitehouse Station, NJ) with chloroform/methanol/4.2 M ammonia (9:7:2, vol/vol) (for detection of complex sphingolipids) or hexane/diethyl ether/acetic acid (30:70:1, vol/vol) (for detection of sterols) as the solvent system. The TLC plates were sprayed with 10% copper sulfate in 8% orthophosphoric acid and then heated at 180°C to visualize lipids. The relative intensity of each lipid band was determined with ImageJ software (National Institutes of Health, Bethesda, MD). Identification of the band of each complex sphingolipid subtype and sterols was performed as described in previous papers (Uemura *et al*., 2014; Tani and Toume, 2015; Yamaguchi *et al*., 2018).

LC-ESI MS/MS analysis of Cers

Lipids were extracted from cells (3 OD_{600} units), subjected to mild alkaline treatment, and then dried as described above. The lipids mainly containing sphingolipids were dissolved in 100 µl of chloroform/methanol/water (5:4:1, vol/vol) with sonication and then mixed with 500 µl of 2-propanol. After centrifugation at 18,000 × *g* for 3 min, 550 µl of the supernatant was transferred to autoinjector vials, and then Cers were measured using LC-ESI MS/MS (3200 QTRAP; SCIEX, USA) equipped with an InertSustain C18 reverse-phase column (2.1 × 150 mm, 5 µm; GL Sciences, Tokyo, Japan). The gradient was started with 40% B (2-propanol with 0.1% formic acid and 0.028% ammonium) in buffer A (acetonitrile/methanol/distilled water, 19:19:2, vol/vol/vol containing 0.1% formic acid and 0.028% ammonium), reached 70% B for 10 min, and maintained at 70% B for 5 min. The gradient was returned to the starting conditions and the column was equilibrated for 5 min before the next run. For the measurement of molecular species of Cers, MRM (multiple reaction monitoring) analysis with positive ion mode was constructed with the combinations LCBs phytosphingosine [t16:0, t18:0, t20:0] or

difference. (D) Efficiency of incorporation of rhodamine 6G into cells under ATP-nondepleted conditions. (E–I) Efficiency of incorporation of rhodamine 6G under stress conditions. Cells (1 OD_{600} units/300 µl) were incubated with 10 µM rhodamine 6G in YPD medium containing 1 M NaCl (E), 2 M sorbitol (F), 0.005% SDS (G), or 300 mM acetic acid (adjusted to pH 5.5 by the addition of 50 mM MES and MOPS) (H) for 30 min. YPD medium buffered at pH 8.0 was prepared by the addition of 100 mM HEPES (I). (J) Evaluation of membrane lipid order by using di-4-ANEPPDHQ. Cells were cultured overnight in YPD medium at 30°C, diluted (0.3 OD_{600} units/ml) in fresh YPD medium, and then incubated for 5 h at 30°C. di-4-ANEPPDHQ (5 µM) was added to cells (1 OD_{600} units/100 µl), followed by incubation for 1 min at 30°C. The ratio of green (525 nm) and red (610 nm) fluorescences in individual cells, which was measured by a flow cytometer, is expressed as a boxplot. Data represent the value for 1000 cells for individual strains. The average (marked as x) of the fluorescence ratio in wild-type cells was taken as 1. (K) Distribution of eisosomes in wild-type and *ccssΔ* cells. Cells expressing Pil1-yeGFP were cultured overnight in YPD medium at 30°C, diluted (0.3 OD_{600} units/ml) in fresh YPD medium, and then incubated for 5 h at 30°C. Cells were observed under a fluorescence microscope. Eisosomes in top section of images of individual cells ($n = 30$) were counted by using Fiji (Schindelin *et al*., 2012; Sakata *et al*., 2022).

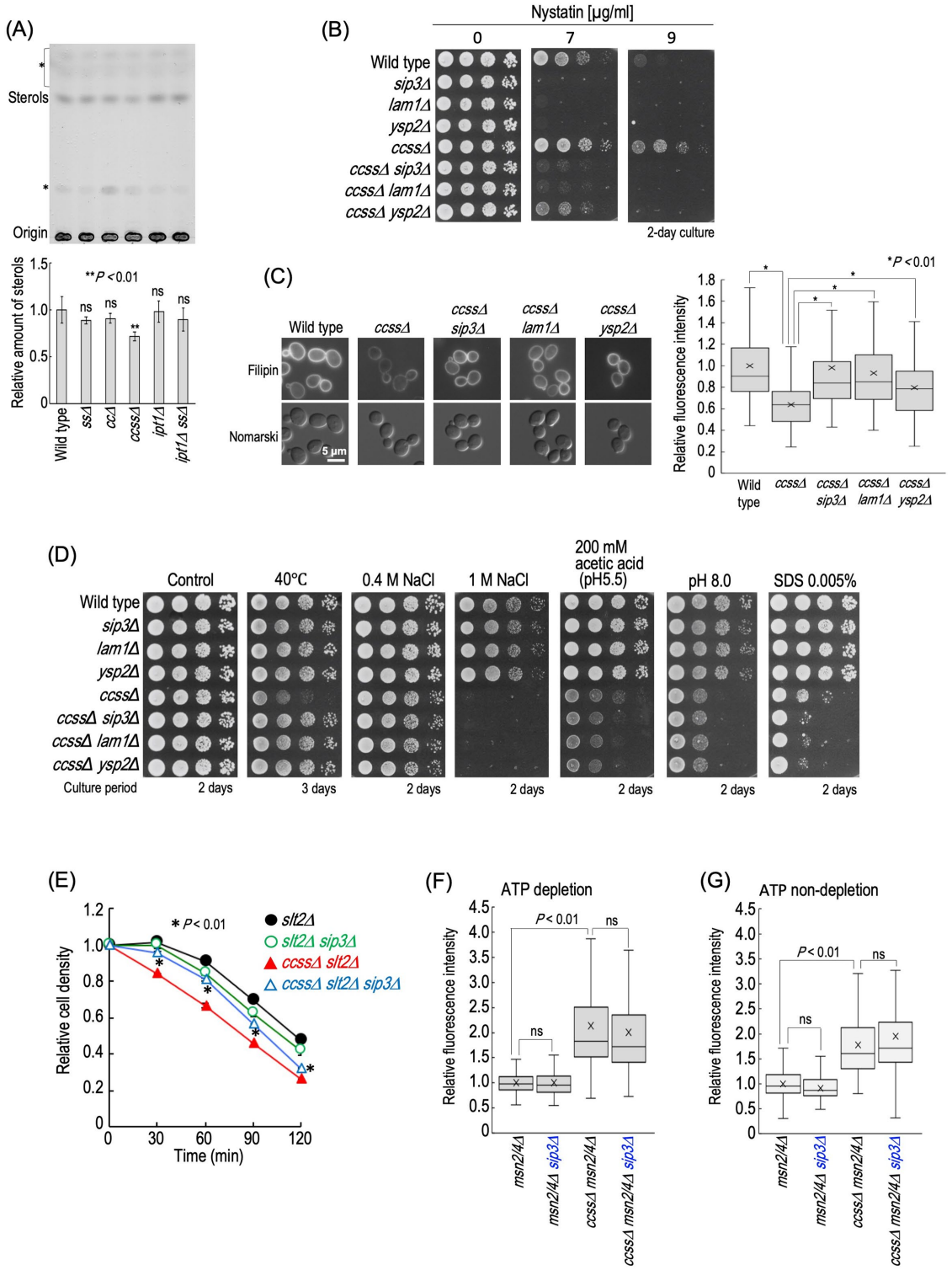

FIGURE 8: Alteration of distribution of sterols at plasma membranes restores impairment of cell wall but not plasma membrane integrity in *ccss*Δ cells. (A) TLC analysis of sterols in wild-type, *ss*Δ, *cc*Δ, *ccss*Δ, *ipt1*Δ, and *ipt1*Δ *ss*Δ cells. Cells were cultured overnight in YPD medium, diluted (0.3 OD_{600} units/ml) in fresh YPD medium, and then incubated for 5 h at 30°C. Lipids were extracted, separated by TLC, and then visualized with a copper sulfate and orthophosphoric acid reagent. The intensity of band of sterols in wild-type cells was taken as 1. Data represent means ± SD for one experiment (triplicate) representative of three independent experiments. ns: no significant difference. The asterisk indicates unidentified bands. (B) Nystatin sensitivity. Cells cultured overnight in YPD medium at 30°C were spotted onto YPD plates containing the indicated concentrations of nystatin and then incubated at 30°C for 2 d. (C) Filipin staining. Cells were cultured overnight in YPD medium, diluted (0.3 OD_{600} units/ml) in fresh YPD medium, and then incubated for 5 h at 30°C. Cells were stained with filipin and observed under a fluorescence microscope. The fluorescence intensity of individual cells is expressed as a boxplot. Data represent the value for 100 cells for individual strains. The average

dihydrosphingosine [d16:0, d18:0, d20:0]), fatty acids with different chain lengths (C16:0, C18:0, C20:0, C22:0, C24:0, or C26:0), and fatty acids with different hydroxylation states (0 [A and B type], 1 [B′ and C type], or 2 [D type]). Collision energy for generating product ion was 35. The peak intensity of each Cer molecular species was analyzed using MultiQuant 3.0.1 (SCIEX).

Yeast protein extraction, SDS–PAGE, and Western blotting

Protein extraction, SDS–PAGE, and Western blotting were performed as described elsewhere (Tani and Kuge, 2010b) with some modifications. For protein extraction, yeast cells (2 OD_{600} units) grown in YPD medium were collected by centrifugation, washed with water, and then resuspended in 100 µl of 0.2 N NaOH containing 0.5% 2-mercaptoethanol. The suspension was incubated on ice for 15 min. One milliliter of ice-cold acetone was added to the suspension, followed by incubation for 30 min at –25°C, and then the proteins were precipitated by centrifugation for 10 min at 10,000 × *g*. The pellet was resuspended in 100 µl of SDS sample buffer (156 mM Tris-HCl, pH 6.8, containing 5% SDS, 25% glycerol, 5% 2-mercaptoethanol and 0.001% bromophenol blue). The suspension was mixed well, heated for 3 min at 95°C, and then centrifuged for 2 min at 10,000 × *g*. Then the supernatant was separated by SDS–PAGE according to the method of Laemmli (1970). For Western blotting, anti-HA (HA-7; Sigma-Aldrich), anti–phospho-p38 MAPK, anti–phospho-p44/42 MAPK (Cell Signaling Technology, Danvers, MA), anti-Hog1 (Santa Cruz Biotechnology, Santa Cruz, CA), and anti-Pgk1 (Thermo Fisher Scientific, Waltham, MA) were used as primary antibodies. Horseradish peroxidase–conjugated anti-mouse or anti-rabbit immunoglobulin G (Thermo Fisher Scientific) was used as the secondary antibody. The relative intensity of each protein band was determined with ImageJ software.

Enzyme assay for α-galactosidase

α-Galactosidase assays were carried out as described previously (Yamaguchi *et al*., 2018) with minor modifications. Briefly, cells (0.7 or 1 OD_{600} units for measurement of 6xSTRE or *NCW2*, *SED1*, and *CRH1* promoters, respectively) were suspended in 200 µl of 20 mM Tris-HCl buffer, pH 7.5, containing 0.35% 2-mercaptoethanol and 0.002% SDS (buffer A), 5 µl of chloroform was added, and then the samples were vortexed for 10 s. For measurement of the activity of α-galactosidase expressed by *NCW2*, *SED1*, and *CRH1* promoters, the samples were diluted 10-fold with buffer A. After 5 min of preincubation at 30°C, the samples (200 µl) were mixed with 80 µl of 7 mM *p*-nitrophenyl-α-galactoside (Sigma-Aldrich) in 100 mM citric acid buffer, pH 4.0, and then incubated at 30°C for 10 min (for 6xSTRE) or 15 min (for *NCW2*, *SED1*, and *CRH1* promoters). Following quenching of the reaction with 900 µl of 0.1 M NaOH, samples were centrifuged at 10,000 × *g* for 1 min, and the A_{410} of the supernatants was measured.

RNA-sequencing

Wild-type (n = 3) and *ccss*Δ (n = 3) cells were cultured overnight in YPD medium, diluted (0.3 OD_{600} units/ml) in fresh YPD medium, and then incubated for 5 h at 30°C. The total RNA was extracted from cells (10 OD_{600} units) by the hot-phenol methods (Collart and Oliviero, 2001) and then purified using the TRIzol LS Reagent (Thermo Fisher Scientific) and an SV Total RNA Isolation System (Promega, Madison, WI) according to the manufacturers' instructions. RNA samples were quantified with an ND-1000 spectrophotometer (NanoDrop Technologies, Wilmington, DE), and the quality was confirmed with a Tapestation (Agilent Technologies, Santa Clara, CA). The sequencing libraries were prepared from 200 ng of total RNA with the NEBNext Magnesium RNA Fragmentation Module (New England Biolab, USA) and the MGIEasy RNA Directional Library Prep Set (MGI, Shenzhen, China) according to the manufacturers' instructions. The libraries were sequenced with a DNBSEQ-G400 FAST Sequencer (MGI) using the paired-end 150 nt strategy. Quality trimming and adapter clipping of the read data were performed using Trimmomatic version 0.38 (Bolger *et al*., 2014). Trimmed reads were mapped to the transcript in the reference S288C (https://www.yeastgenome.org/strain/s288c) using the Bowtie2 aligner within RSEM (RNA-Seq by expectation-maximization) (Li and Dewey, 2011). The abundance estimation for genes and isoforms with RSEM generated basic counts data (expected counts). The edgeR (Robinson *et al*., 2010) program was used to detect the differentially expressed genes (DEGs). Normalized counts per million (CPM) values, log fold changes (logFC), and P values were obtained from the normalized CPM values. Then criteria for DEGs were established: P value ≤ 0.01 and fold change ≥1.4. The data sets of RNA-sequencing are listed in Supplemental Table S1.

Translocation of yeGFP-Rim101 into nuclei

Cells were collected by centrifugation, fixed with 500 µl of 2% paraformaldehyde in phosphate-buffered saline (PBS) (–), and then incubated at room temperature for 30 min. Cells were washed twice with PBS (–) and then viewed under a fluorescence microscope. For quantification of the nuclear localization of yeGFP-Rim101, the fixed cells were stained with 10 µg/ml 4′,6-diamidino-2-phenylindole (Dojindo Chemical Laboratories, Kumamoto, Japan) for 30 min. The fluorescence intensity of yeGFP in cytoplasm and the nucleus in individual cells was quantified with ImageJ software.

Rhodamine 6G incorporation into cells

Cells were cultured overnight in YPD medium, diluted (0.3 OD_{600} units/ml) in fresh YPD medium, and then incubated for 5 h at 30°C. For measurement of the incorporation rate of rhodamine 6G under ATP-depleted conditions, cells (1 OD_{600} units) were preincubated in 300 µl of YP (1% yeast extract and 2% peptone) containing 50 mM 2-deoxy-D-glucose (Nacalai Tesque) and 10 mM NaN_3 and NaF for 30 min at 30°C and then incubated with 10 µM rhodamine 6G (Tokyo Chemical Industry, Tokyo, Japan) for 30 min at 30°C. When ATP was not depleted, cells (1 OD_{600} units) were resuspended in 300 µl of YPD medium containing 10 µM rhodamine 6G and then incubated for 30 min at 30°C. The cells were collected by centrifugation, washed with 10 mM NaN_3 and NaF, and then viewed under a fluorescence microscope. The fluorescence intensity of rhodamine 6G in individual cells was quantified with ImageJ software.

(marked as x) of fluorescence intensity in wild-type cells was taken as 1. (D) Effects of deletion of *SIP3*, *LAM1*, or *YSP2* on stress sensitivities. Cells cultured overnight in YPD medium were spotted onto YPD plates (the details of the composition of the medium are given in Figure 2). Plates were incubated at 30 or 40°C for the indicated numbers of days. (E) The zymolyase sensitivities of *slt2*Δ, *slt2*Δ *sip3*Δ, *ccss*Δ *slt2*Δ, and *ccss*Δ *slt2*Δ *sip3*Δ cells were examined as described in Figure 6E. (F, G) The efficiency of rhodamine 6G incorporation into *msn2/4*Δ, *msn2/4*Δ *sip3*Δ, *ccss*Δ *msn2/4*Δ, and *ccss*Δ *msn2/4*Δ *sip3*Δ under ATP-depleted (F) or ATP-nondepleted (G) conditions was examined as described in Figure 7. The details are given in *Materials and Methods*.

Strain	Genotype	Source
BY4741	*MATa his3Δ1 leu2Δ0 met15Δ0 ura3Δ0*	Brachmann *et al.*, 1998
MTY174	BY4741, *URA3*	Arita *et al.*, 2020
MTY128	BY4741, *sur2Δ::URA3*	Tani and Kuge, 2012a
MTY211	BY4741, *scs7Δ::URA3*	Tani and Kuge, 2012a
AKY55	BY4741, *sur2Δ::kanMX4 scs7Δ::URA3*	This study
AKY56	BY4741, *csg1Δ::natMX4 csh1Δ::URA3*	This study
AKY57	BY4741, *csg1Δ::natMX4 csh1Δ::hphNT1 sur2Δ::URA3*	This study
AKY58	BY4741, *csg1Δ::natMX4 csh1Δ::hphNT1 scs7Δ::URA3*	This study
AKY59	BY4741, *csg1Δ::natMX4 csh1Δ::hphNT1 sur2Δ:URA3 scs7Δ::kanMX4*	This study
AKY61	BY4741, *ipt1Δ::URA3*	This study
AKY62	BY4741, *ipt1Δ::URA3 sur2Δ::kanMX4*	This study
AKY63	BY4741, *ipt1Δ::URA3 scs7Δ::hphNT1*	This study
AKY64	BY4741, *ipt1Δ::URA3 sur2Δ::kanMX4 scs7Δ::hphNT1*	This study
AKY75	BY4741, *hog1Δ::LEU2 URA3*	This study
AKY80	BY4741, *sur2Δ::kanMX4 scs7Δ::URA3 hog1Δ::LEU2*	This study
AKY83	BY4741, *csg1Δ::natMX4 csh1Δ::URA3 hog1Δ::LEU2*	This study
AKY86	BY4741, *csg1Δ::natMX4 csh1Δ::hphNT1 sur2Δ:URA3 scs7Δ::kanMX4 hog1Δ::LEU2*	This study
AKY76	BY4741, *slt2Δ::LEU2 URA3*	This study
AKY78	BY4741, *sur2Δ::kanMX4 scs7Δ::URA3 slt2Δ::LEU2*	This study
AKY85	BY4741, *csg1Δ::natMX4 csh1Δ::URA3 slt2Δ::LEU2*	This study
MTY2884	BY4741, *csg1Δ::natMX4 csh1Δ::hphNT1 sur2Δ:URA3 scs7Δ::kanMX4 slt2Δ::LEU2*	This study
MTY2886	BY4741, *rim101Δ::LEU2 URA3*	This study
AKY109	BY4741, *sur2Δ::URA3 scs7Δ::LEU2 rim101Δ::natNT2*	This study
AKY111	BY4741, *csg1Δ::URA3 csh1Δ::LEU2 rim101Δ::natNT2*	This study
MTY2885	BY4741, *csg1Δ::natMX4 csh1Δ::hphNT1 sur2Δ:URA3 scs7Δ::kanMX4 rim101Δ::LEU2*	This study
MTY2941	BY4741, *SLT2-6xHA::hphNT1 URA3 LEU2*	This study
AKY275	BY4741, *csg1Δ::URA3 csh1Δ::LEU2 sur2Δ::kanMX4 scs7Δ::natNT2 SLT2-6HA::hphNT1*	This study
AKY280	BY4741, *TEFp-yeGFP-RIM101::natNT2 URA3 LEU2*	This study
AKY283	BY4741, *csg1Δ::URA3 csh1Δ::LEU2 sur2Δ::kanMX4 scs7Δ::hphNT1 TEFp-yeGFP-RIM101::natNT2*	This study
AKY312	BY4741, *msn2Δ::HIS3 msn4Δ::LEU2 URA3*	This study
AKY127	BY4741, *sur2Δ::kanMX4 scs7Δ::URA3 msn2Δ::HIS3 msn4Δ::LEU2*	This study
AKY316	BY4741, *csg1Δ::natMX4 csh1Δ::hphNT1 msn2Δ::HIS3 msn4Δ::LEU2 URA3*	This study
MTY2957	BY4741, *csg1Δ::natMX4 csh1Δ::hphNT1 sur2Δ::URA3 scs7Δ::kanMX4 msn2Δ::HIS3 msn4Δ::LEU2*	This study
AKY244	BY4741, *LEU2* harboring pRS416-*6xSTRE-MEL1*	This study
AKY247	BY4741, *csg1Δ::natMX4 csh1Δ::hphNT1 sur2Δ::kanMX4 scs7Δ::LEU2* harboring pRS416-*6xSTRE-MEL1*	This study
AKY248	BY4741, *msn2Δ::natNT2 msn4Δ::hphMX4* harboring pRS416-*6xSTRE-MEL1*	This study
AKY249	BY4741, *csg1Δ::natMX4 csh1Δ::hphNT1 sur2Δ::LEU2 scs7Δ::kanMX4 msn2Δ::HIS3 msn4Δ::MET15* harboring pRS416-*6xSTRE-MEL1*	This study
MTY3090	BY4741, *bck1Δ::hphNT1 URA3*	This study
MTY3091	BY4741, *csg1Δ::natMX4 csh1Δ::URA3 bck1Δ::hphNT1*	This study
MTY3092	BY4741, *csg1Δ::URA3 csh1Δ::LEU2 sur2Δ::kanMX4 scs7Δ::natNT2 bck1Δ::hphNT1*	This study

TABLE 1: Strains used in this study.

(*Continues*)

Strain	Genotype	Source
MTY3093	BY4741, *rom2Δ::hphNT1 URA3*	This study
MTY3094	BY4741, *csg1Δ::natMX4 csh1Δ::URA3 rom2Δ::hphNT1*	This study
MTY3089	BY4741, *csg1Δ::URA3 csh1Δ::LEU2 sur2Δ::kanMX4 scs7Δ::natNT2 rom2Δ::hphNT1*	This study
MTY3097	BY4741 harboring pRS415-*NCW2p-MEL1*	This study
MTY3098	BY4741, *slt2Δ::hphMX4* harboring pRS415-*NCW2p-MEL1*	This study
MTY3099	BY4741, *csg1Δ::natMX4 csh1Δ::hphNT1 sur2Δ:URA3 scs7Δ::kanMX4* harboring pRS415-*NCW2p-MEL1*	This study
MTY3100	BY4741, *csg1Δ::natMX4 csh1Δ::hphNT1 sur2Δ:URA3 scs7Δ::kanMX4 slt2Δ::MET15* harboring pRS415-*NCW2p-MEL1*	This study
MTY3101	BY4741 harboring pRS415-*SED1p-MEL1*	This study
MTY3102	BY4741, *slt2Δ::hphMX4* harboring pRS415-*SED1p-MEL1*	This study
MTY3103	BY4741, *csg1Δ::natMX4 csh1Δ::hphNT1 sur2Δ:URA3 scs7Δ::kanMX4* harboring pRS415-*SED1p-MEL1*	This study
MTY3104	BY4741, *csg1Δ::natMX4 csh1Δ::hphNT1 sur2Δ:URA3 scs7Δ::kanMX4 slt2Δ::MET15* harboring pRS415-*SED1p-MEL1*	This study
MTY3105	BY4741 harboring pRS415-*CRH1p-MEL1*	This study
MTY3106	BY4741, *slt2Δ::hphMX4* harboring pRS415-*CRH1p-MEL1*	This study
MTY3107	BY4741, *csg1Δ::natMX4 csh1Δ::hphNT1 sur2Δ:URA3 scs7Δ::kanMX4* harboring pRS415-*CRH1p-MEL1*	This study
MTY3108	BY4741, *csg1Δ::natMX4 csh1Δ::hphNT1 sur2Δ:URA3 scs7Δ::kanMX4 slt2Δ::MET15* harboring pRS415-*CRH1p-MEL1*	This study
STY89	BY4741, *erg6Δ::kanMX4*	Tanaka and Tani, 2018
MTY3095	BY4741, *PIL1-yeGFP::hphNT1 URA3*	This study
MTY3096	BY4741, *csg1Δ::URA3 csh1Δ::LEU2 sur2Δ::kanMX4 scs7Δ::natNT2 PIL1-yeGFP::hphNT1*	This study
MTY2297	BY4741, *sip3Δ::kanMX4*	Otsu *et al.*, 2020
MTY2300	BY4741, *lam1Δ::kanMX4*	Otsu *et al.*, 2020
MTY2338	BY4741, *ysp2Δ::kanMX4*	Otsu et al., 2020
AKY260	BY4741, *csg1Δ::URA3 csh1Δ::HIS3 sur2Δ::kanMX4 scs7Δ::hphNT1 sip3Δ::natNT2*	This study
AKY261	BY4741, *csg1Δ::URA3 csh1Δ::HIS3 sur2Δ::kanMX4 scs7Δ::hphNT1 lam1Δ::natNT2*	This study
AKY262	BY4741, *csg1Δ::URA3 csh1Δ::HIS3 sur2Δ::kanMX4 scs7Δ::hphNT1 ysp2Δ::natNT2*	This study
AKY318	BY4741, *slt2Δ::LEU2 sip3Δ::kanMX4*	This study
MTY3003	BY4741, *csg1Δ::URA3 csh1Δ::HIS3 sur2Δ::kanMX4 scs7Δ::hphNT1 slt2Δ::LEU2 sip3Δ::natNT2*	This study
MTY3000	BY4741, *msn2Δ::HIS3 msn4Δ::LEU2 sip3Δ::kanMX4 URA3*	This study
MTY3007	BY4741, *csg1Δ::URA3 csh1Δ::HIS3 sur2Δ::kanMX4 scs7Δ::hphNT1 msn2Δ::LEU2 msn4Δ::MET15 sip3Δ::natNT2*	This study

TABLE 1: Strains used in this study. Continued

di-4-ANEPPDHQ staining

di-4-ANEPPDHQ staining of yeast cells was performed as described in Owen *et al.* (2011) with several modifications. Briefly, cells (1 OD_{600} units) were suspended in 100 µl of YPD medium containing 5 µM di-4-ANEPPDHQ and incubated for 1 min at 30°C, and then measurement of the intensity of green fluorescence (emission wavelength of 525 ± 20 nm) and red fluorescence (emission wavelength of 610 ± 10 nm), which were excited at 488 nm, was performed by flow cytometry.

Filipin staining

Filipin staining of yeast cells was performed as described in Nakase *et al.* (2010). Briefly, filipin was added to the medium at a final concentration of 15 µg/ml, and cells were observed immediately using a fluorescence microscope.

Statistical analysis

Statistical analysis was performed using Student's *t* test, and the *P* values obtained are indicated.

ACKNOWLEDGMENTS

We thank O. Kuge, T. Ogishima, and N. Miyata (Kyushu University) for valuable suggestions regarding this study. This study was supported by KAKENHI (21H02118) from the Ministry of Education, Culture, Sports, Science, and Technology, Japan, the Noda Institute for Scientific Research, Japan, and the Ohsumi Frontier Science Foundation, Japan.

REFERENCES

Abe F, Hiraki T (2009). Mechanistic role of ergosterol in membrane rigidity and cycloheximide resistance in Saccharomyces cerevisiae. Biochim Biophys Acta 1788, 743–752.

Arita N, Sakamoto R, Tani M (2020). Mitochondrial reactive oxygen species-mediated cytotoxicity of intracellularly accumulated dihydrosphingosine in the yeast Saccharomyces cerevisiae. FEBS J 287, 3427–3448.

Beeler TJ, Fu D, Rivera J, Monaghan E, Gable K, Dunn TM (1997). SUR1 (CSG1/BCL21), a gene necessary for growth of Saccharomyces cerevisiae in the presence of high Ca2+ concentrations at 37 degrees C, is required for mannosylation of inositolphosphorylceramide. Mol Gen Genet 255, 570–579.

Berchtold D, Piccolis M, Chiaruttini N, Riezman I, Riezman H, Roux A, Walther TC, Loewith R (2012). Plasma membrane stress induces relocalization of Slm proteins and activation of TORC2 to promote sphingolipid synthesis. Nat Cell Biol 14, 542–547.

Bolger AM, Lohse M, Usadel B (2014). Trimmomatic: a flexible trimmer for Illumina sequence data. Bioinformatics 30, 2114–2120.

Brachmann CB, Davies A, Cost GJ, Caputo E, Li J, Hieter P, Boeke JD (1998). Designer deletion strains derived from Saccharomyces cerevisiae S288C: a useful set of strains and plasmids for PCR-mediated gene disruption and other applications. Yeast 14, 115–132.

Brewster JL, Gustin MC (2014). Hog1: 20 years of discovery and impact. Sci Signal 7, re7.

Chung N, Mao C, Heitman J, Hannun YA, Obeid LM (2001). Phytosphingosine as a specific inhibitor of growth and nutrient import in Saccharomyces cerevisiae. J Biol Chem 276, 35614–35621.

Clay L, Caudron F, Denoth-Lippuner A, Boettcher B, Buvelot Frei S, Snapp EL, Barral Y (2014). A sphingolipid-dependent diffusion barrier confines ER stress to the yeast mother cell. eLife 3, e01883.

Collart MA, Oliviero S (2001). Preparation of yeast RNA. Curr Protoc Mol Biol Chapter 13, Unit13.12.

Dickson RC, Lester RL (2002). Sphingolipid functions in Saccharomyces cerevisiae. Biochim Biophys Acta 1583, 13–25.

Dickson RC, Nagiec EE, Wells GB, Nagiec MM, Lester RL (1997). Synthesis of mannose-(inositol-P)2-ceramide, the major sphingolipid in Saccharomyces cerevisiae, requires the IPT1 (YDR072c) gene. J Biol Chem 272, 29620–29625.

Dickson RC, Sumanasekera C, Lester RL (2006). Functions and metabolism of sphingolipids in Saccharomyces cerevisiae. Prog Lipid Res 45, 447–465.

Dudley AM, Janse DM, Tanay A, Shamir R, Church GM (2005). A global view of pleiotropy and phenotypically derived gene function in yeast. Mol Syst Biol 1, 2005.0001.

Dupont S, Beney L, Ritt JF, Lherminier J, Gervais P (2010). Lateral reorganization of plasma membrane is involved in the yeast resistance to severe dehydration. Biochim Biophys Acta 1798, 975–985.

Ejsing CS, Sampaio JL, Surendranath V, Duchoslav E, Ekroos K, Klemm RW, Simons K, Shevchenko A (2009). Global analysis of the yeast lipidome by quantitative shotgun mass spectrometry. Proc Natl Acad Sci USA 106, 2136–2141.

Frohlich F, Moreira K, Aguilar PS, Hubner NC, Mann M, Walter P, Walther TC (2009). A genome-wide screen for genes affecting eisosomes reveals Nce102 function in sphingolipid signaling. J Cell Biol 185, 1227–1242.

Futai E, Maeda T, Sorimachi H, Kitamoto K, Ishiura S, Suzuki K (1999). The protease activity of a calpain-like cysteine protease in Saccharomyces cerevisiae is required for alkaline adaptation and sporulation. Mol Gen Genet 260, 559–568.

Gasch AP, Spellman PT, Kao CM, Carmel-Harel O, Eisen MB, Storz G, Botstein D, Brown PO (2000). Genomic expression programs in the response of yeast cells to environmental changes. Mol Biol Cell 11, 4241–4257.

Gatta AT, Wong LH, Sere YY, Calderon-Norena DM, Cockcroft S, Menon AK, Levine TP (2015). A new family of StART domain proteins at membrane contact sites has a role in ER-PM sterol transport. eLife 4, e07253.

Guan XL, Souza CM, Pichler H, Dewhurst G, Schaad O, Kajiwara K, Wakabayashi H, Ivanova T, Castillon GA, Piccolis M, *et al.* (2009). Functional interactions between sphingolipids and sterols in biological membranes regulating cell physiology. Mol Biol Cell 20, 2083–2095.

Haak D, Gable K, Beeler T, Dunn T (1997). Hydroxylation of Saccharomyces cerevisiae ceramides requires Sur2p and Scs7p. J Biol Chem 272, 29704–29710.

Hallstrom TC, Lambert L, Schorling S, Balzi E, Goffeau A, Moye-Rowley WS (2001). Coordinate control of sphingolipid biosynthesis and multidrug resistance in Saccharomyces cerevisiae. J Biol Chem 276, 23674–23680.

Hanson BA, Lester RL (1980). The extraction of inositol-containing phospholipids and phosphatidylcholine from Saccharomyces cerevisiae and Neurospora crassa. J Lipid Res 21, 309–315.

Hechtberger P, Zinser E, Saf R, Hummel K, Paltauf F, Daum G (1994). Characterization, quantification and subcellular localization of inositol-containing sphingolipids of the yeast, Saccharomyces cerevisiae. Eur J Biochem 225, 641–649.

Herrero AB, Astudillo AM, Balboa MA, Cuevas C, Balsinde J, Moreno S (2008). Levels of SCS7/FA2H-mediated fatty acid 2-hydroxylation determine the sensitivity of cells to antitumor PM02734 . Cancer Res 68, 9779–9787.

Imazu H, Sakurai H (2005). Saccharomyces cerevisiae heat shock transcription factor regulates cell wall remodeling in response to heat shock. Eukaryot Cell 4, 1050–1056.

Khmelinskaia A, Marques JMT, Bastos AEP, Antunes CAC, Bento-Oliveira A, Scolari S, Lobo G, Malho R, Herrmann A, Marinho HS, de Almeida RFM (2020). Liquid-ordered phase formation by mammalian and yeast sterols: a common feature with organizational differences. Front Cell Dev Biol 8, 337.

Kishimoto T, Mioka T, Itoh E, Williams DE, Andersen RJ, Tanaka K (2021). Phospholipid flippases and Sfk1 are essential for the retention of ergosterol in the plasma membrane. Mol Biol Cell 32, 1374–1392.

Knupp J, Martinez-Montanes F, Van Den Bergh F, Cottier S, Schneiter R, Beard D, Chang A (2017). Sphingolipid accumulation causes mitochondrial dysregulation and cell death. Cell Death Differ 24, 2044–2053.

Kono K, Al-Zain A, Schroeder L, Nakanishi M, Ikui AE (2016). Plasma membrane/cell wall perturbation activates a novel cell cycle checkpoint during G1 in Saccharomyces cerevisiae. Proc Natl Acad Sci USA 113, 6910–6915.

Laemmli UK (1970). Cleavage of structural proteins during the assembly of the head of bacteriophage T4. Nature 227, 680–685.

Leskoske KL, Roelants FM, Emmerstorfer-Augustin A, Augustin CM, Si EP, Hill JM, Thorner J (2018). Phosphorylation by the stress-activated MAPK Slt2 down-regulates the yeast TOR complex 2. Genes Dev 32, 1576–1590.

Levin DE (2005). Cell wall integrity signaling in Saccharomyces cerevisiae. Microbiol Mol Biol Rev 69, 262–291.

Li B, Dewey CN (2011). RSEM: accurate transcript quantification from RNA-Seq data with or without a reference genome. BMC Bioinformatics 12, 323.

Lindahl L, Genheden S, Eriksson LA, Olsson L, Bettiga M (2016). Sphingolipids contribute to acetic acid resistance in Zygosaccharomyces bailii. Biotechnol Bioeng 113, 744–753.

Luo G, Gruhler A, Liu Y, Jensen ON, Dickson RC (2008). The sphingolipid long-chain base-Pkh1/2-Ypk1/2 signaling pathway regulates eisosome assembly and turnover. J Biol Chem 283, 10433–10444.

Martinez-Arias A, Yost HJ, Casadaban MJ (1984). Role of an upstream regulatory element in leucine repression of the Saccharomyces cerevisiae leu2 gene. Nature 307, 740–742.

Merrill AH Jr (2011). Sphingolipid and glycosphingolipid metabolic pathways in the era of sphingolipidomics. Chem Rev 111, 6387–6422.

Mioka T, Fujimura-Kamada K, Mizugaki N, Kishimoto T, Sano T, Nunome H, Williams DE, Andersen RJ, Tanaka K (2018). Phospholipid flippases and Sfk1p, a novel regulator of phospholipid asymmetry, contribute to low permeability of the plasma membrane. Mol Biol Cell 29, 1203–1218.

Mira NP, Palma M, Guerreiro JF, Sa-Correia I (2010). Genome-wide identification of Saccharomyces cerevisiae genes required for tolerance to acetic acid. Microb Cell Fact 9, 79.

Morimoto Y, Tani M (2015). Synthesis of mannosylinositol phosphorylceramides is involved in maintenance of cell integrity of yeast Saccharomyces cerevisiae. Mol Microbiol 95, 706–722.

Moskvina E, Schuller C, Maurer CT, Mager WH, Ruis H (1998). A search in the genome of Saccharomyces cerevisiae for genes regulated via stress response elements. Yeast 14, 1041–1050.

Nakase M, Tani M, Morita T, Kitamoto HK, Kashiwazaki J, Nakamura T, Hosomi A, Tanaka N, Takegawa K (2010). Mannosylinositol phosphorylceramide is a major sphingolipid component and is required for proper localization of plasma-membrane proteins in Schizosaccharomyces pombe. J Cell Sci 123, 1578–1587.

Otsu M, Toume M, Yamaguchi Y, Tani M (2020). Proper regulation of inositolphosphorylceramide levels is required for acquirement of low pH resistance in budding yeast. Sci Rep 10, 10792.

Owen DM, Rentero C, Magenau A, Abu-Siniyeh A, Gaus K (2011). Quantitative imaging of membrane lipid order in cells and organisms. Nat Protoc 7, 24–35.

Petelenz-Kurdziel E, Eriksson E, Smedh M, Beck C, Hohmann S, Goksor M (2011). Quantification of cell volume changes upon hyperosmotic stress in Saccharomyces cerevisiae. Integr Biol 3, 1120–1126.
Pina F, Yagisawa F, Obara K, Gregerson JD, Kihara A, Niwa M (2018). Sphingolipids activate the endoplasmic reticulum stress surveillance pathway. J Cell Biol 217, 495–505.
Ram AF, Klis FM (2006). Identification of fungal cell wall mutants using susceptibility assays based on Calcofluor white and Congo red. Nat Protoc 1, 2253–2256.
Robinson MD, McCarthy DJ, Smyth GK (2010). edgeR: a bioconductor package for differential expression analysis of digital gene expression data. Bioinformatics 26, 139–140.
Roelants FM, Leskoske KL, Martinez Marshall MN, Locke MN, Thorner J (2017). The TORC2-dependent signaling network in the yeast Saccharomyces cerevisiae. Biomolecules 7, 66.
Sakata KT, Hashii K, Yoshizawa K, Tahara YO, Yae K, Tsuda R, Tanaka N, Maeda T, Miyata M, Tabuchi M (2022). Coordinated regulation of TORC2 signaling by MCC/eisosome-associated proteins, Pil1 and tetraspan membrane proteins during the stress response. Mol Microbiol 117, 1227–1244.
Schindelin J, Arganda-Carreras I, Frise E, Kaynig V, Longair M, Pietzsch T, Preibisch S, Rueden C, Saalfeld S, Schmid B, *et al*. (2012). Fiji: an open-source platform for biological-image analysis. Nat Methods 9, 676–682.
Schmitt AP, McEntee K (1996). Msn2p, a zinc finger DNA-binding protein, is the transcriptional activator of the multistress response in Saccharomyces cerevisiae. Proc Natl Acad Sci USA 93, 5777–5782.
Serhan G, Stack CM, Perrone GG, Morton CO (2014). The polyene antifungals, amphotericin B and nystatin, cause cell death in Saccharomyces cerevisiae by a distinct mechanism to amphibian-derived antimicrobial peptides. Ann Clin Microbiol Antimicrob 13, 18.
Slotte JP (2016). The importance of hydrogen bonding in sphingomyelin's membrane interactions with co-lipids. Biochim Biophys Acta 1858, 304–310.
Tanaka S, Tani M (2018). Mannosylinositol phosphorylceramides and ergosterol coodinately maintain cell wall integrity in the yeast Saccharomyces cerevisiae. FEBS J 285, 2405–2427.
Tani M (2016). Structure-function relationship of complex sphingolipids in yeast. Trends Glycosci Glycotechnol 28, E109–E116.
Tani M, Kuge O (2010a). Defect of synthesis of very long-chain fatty acids confers resistance to growth inhibition by inositol phosphorylceramide synthase repression in yeast Saccharomyces cerevisiae. J Biochem 148, 565–571.
Tani M, Kuge O (2010b). Requirement of a specific group of sphingolipid-metabolizing enzyme for growth of yeast Saccharomyces cerevisiae under impaired metabolism of glycerophospholipids. Mol Microbiol 78, 395–413.
Tani M, Kuge O (2012a). Hydroxylation state of fatty acid and long-chain base moieties of sphingolipid determine the sensitivity to growth inhibition due to AUR1 repression in Saccharomyces cerevisiae. Biochem Biophys Res Commun 417, 673–678.
Tani M, Kuge O (2012b). Involvement of complex sphingolipids and phosphatidylserine in endosomal trafficking in yeast Saccharomyces cerevisiae. Mol Microbiol 86, 1262–1280.
Tani M, Toume M (2015). Alteration of complex sphingolipid composition and its physiological significance in yeast Saccharomyces cerevisiae lacking vacuolar ATPase. Microbiology 161, 2369–2383.
Tanigawa M, Kihara A, Terashima M, Takahara T, Maeda T (2012). Sphingolipids regulate the yeast high-osmolarity glycerol response pathway. Mol Cell Biol32, 2861–2870.
Toda T, Urita A, Koga A, Takayama C, Tani M (2020). ROS-mediated synthetic growth defect caused by impaired metabolism of sphingolipids and phosphatidylserine in budding yeast. Biosci Biotechnol Biochem 84, 2529–2532.
Toume M, Tani M (2016). Yeast lacking the amphiphysin-family protein Rvs167 are sensitive to disruptions in sphingolipid levels. FEBS J 283, 2911–2928.
Uemura S, Kihara A, Inokuchi J, Igarashi Y (2003). Csg1p and newly identified Csh1p function in mannosylinositol phosphorylceramide synthesis by interacting with Csg2p. J Biol Chem 278, 45049–45055.
Uemura S, Shishido F, Tani M, Mochizuki T, Abe F, Inokuchi JI (2014). Loss of hydroxyl groups from the ceramide moiety can modify the lateral diffusion of membrane proteins in S. cerevisiae. J Lipid Res 55, 1343–1356.
Urita A, Ishibashi Y, Kawaguchi R, Yanase Y, Tani M (2022). Crosstalk between protein kinase A and the HOG pathway under impaired biosynthesis of complex sphingolipids in budding yeast. FEBS J 289, 766–786.
Walther TC, Aguilar PS, Frohlich F, Chu F, Moreira K, Burlingame AL, Walter P (2007). Pkh-kinases control eisosome assembly and organization. EMBO J 26, 4946–4955.
Wei M, Fabrizio P, Hu J, Ge H, Cheng C, Li L, Longo VD (2008). Life span extension by calorie restriction depends on Rim15 and transcription factors downstream of Ras/PKA, Tor, and Sch9. PLoS Genet 4, e13.
Yabuki Y, Ikeda A, Araki M, Kajiwara K, Mizuta K, Funato K (2019). Sphingolipid/Pkh1/2-TORC1/Sch9 signaling regulates ribosome biogenesis in tunicamycin-induced stress response in yeast. Genetics 212, 175–186.
Yamagata M, Obara K, Kihara A (2013). Unperverted synthesis of complex sphingolipids is essential for cell survival under nitrogen starvation. Genes Cells 18, 650–659.
Yamaguchi Y, Katsuki Y, Tanaka S, Kawaguchi R, Denda H, Ikeda T, Funato K, Tani M (2018). Protective role of the HOG pathway against the growth defect caused by impaired biosynthesis of complex sphingolipids in yeast Saccharomyces cerevisiae. Mol Microbiol 107, 363–386.
Yamashita T, Hashiramoto A, Haluzik M, Mizukami H, Beck S, Norton A, Kono M, Tsuji S, Daniotti JL, Werth N, *et al*. (2003). Enhanced insulin sensitivity in mice lacking ganglioside GM3. Proc Natl Acad Sci USA 100, 3445–3449.
Yoshikawa M, Go S, Takasaki K, Kakazu Y, Ohashi M, Nagafuku M, Kabayama K, Sekimoto J, Suzuki S, Takaiwa K, *et al*. (2009). Mice lacking ganglioside GM3 synthase exhibit complete hearing loss due to selective degeneration of the organ of Corti. Proc Natl Acad Sci USA 106, 9483–9488.
Zhao C, Beeler T, Dunn T (1994). Suppressors of the Ca(2+)-sensitive yeast mutant (csg2) identify genes involved in sphingolipid biosynthesis. Cloning and characterization of SCS1, a gene required for serine palmitoyltransferase activity. J Biol Chem 269, 21480–21488.
Zhao F, Yang J, Li J, Li Z, Lin Y, Zheng S, Liang S, Han S (2020). Multiple cellular responses guarantee yeast survival in presence of the cell membrane/wall interfering agent sodium dodecyl sulfate. Biochem Biophys Res Commun 527, 276–282.